NASA Contractor Report 4550
DOT/FAA/RD-93/24

Designing Clutter Rejection Filters With Complex Coefficients for Airborne Pulsed Doppler Weather Radar

Dennis A. Jamora
Clemson University
Clemson, South Carolina

Prepared for
Langley Research Center
under Grant NAG1-928

National Aeronautics and
Space Administration
Office of Management
Scientific and Technical
Information Program
1993

PAGE INTENTIONALLY BLANK

TABLE OF CONTENTS

Table of Contents (Continued)

LIST OF FIGURES

INTENTIONALLY BLANK

ACKNOWLEDGMENTS

The author would like to express his sincere gratitude to all of those whose help during his graduate studies made this completion possible. First of all is his thesis advisor, Dr. E. G. Baxa, Jr., whose advice and support were instumental during the research and writing for this thesis. Also to be acknowledged are the other members of his commitee, Dr. J. J. Komo and Dr. C. B. Russell, for their time and support. The National Aeronautics and Space Administration is also recognized for their financial support under grant No. NAG-1-928 and for their technical support specifically from the Antenna and Microwave Research Branch at Langley Research Center.

The author is also grateful to the students of the Radar Systems Laboratory at Clemson University for their help and advice and for their willingness to offer their time to assist him. Finally, the author wishes to recognize his family, whose love and support kept him encouraged to complete his studies.

CHAPTER 1

INTRODUCTION

The principle of radar is based on the transmission of electromagnetic energy and the reception of the echo returned from a reflective object, commonly known as a target [1]. By examining the echo signal, it is possible to determine several characteristics of the target. The direction of the target can be determined by using a directive antenna which can sense the arrival angle of the echo signal. The range to a target can be measured by the amount of time it takes the transmitted signal to travel to and from the target. The velocity of the target can be measured based on the Doppler principle. Even the target's size and shape can be determined by the amount of power in the echo signal. The amount of power in the received echo is proportional to the radar cross section (RCS) of the target which is dependent on the target's size, shape and orientation.

Although radar can be operated by transmitting a continuous wave (CW) of electromagnetic energy, the most common form of radar employs a pulsed wave. CW radar necessitates the use of separate antennas for transmission and reception since the transmitter is never off. Also, since the receiver is designed to be sensitive to low power signals, sufficient isolation between the transmitter and receiver is necessary in order to protect the receiver from the high power signal of the transmitter. An unmodulated CW radar cannot measure range based on the time of signal travel since there are no breaks in the signal to indicate the start or end of the signal.

The block diagram in Figure 1.1 shows a simplified pulsed radar system. The duplexer switches between the transmitter and the receiver in order to protect the receiver when the transmitter is on. The transmitter is essentially a high power amplifier which amplifies the waveform generated by the oscillator. The advantage of

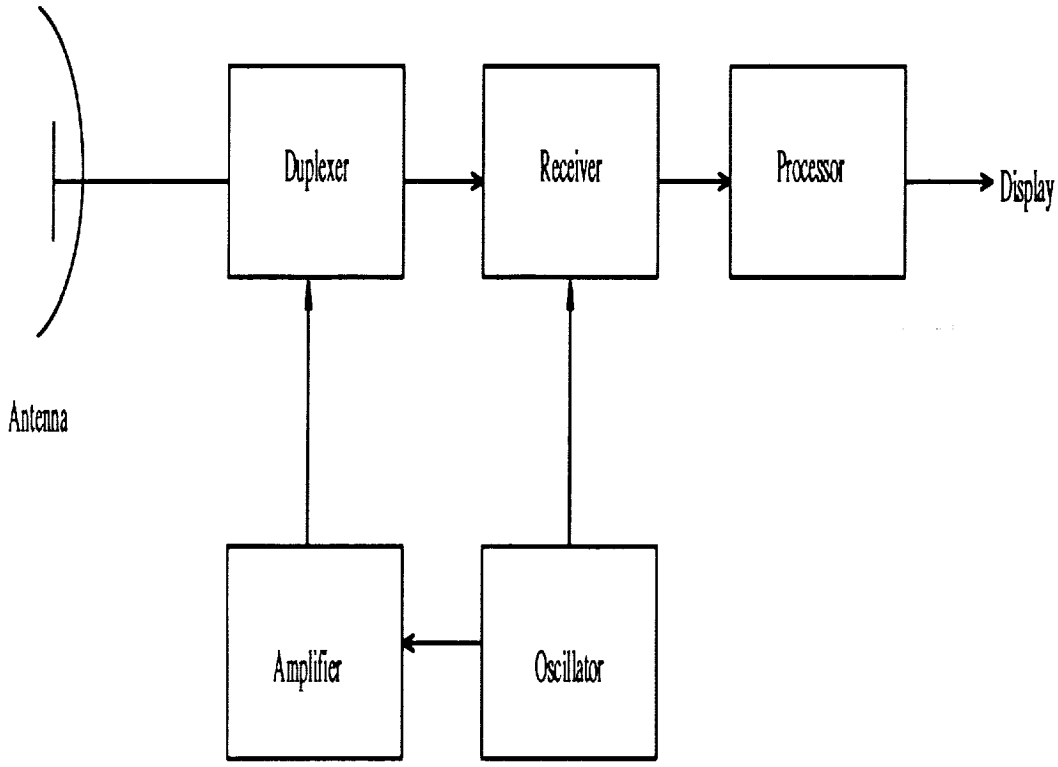

Figure 1.1 Simplified Radar System

a pulsed system is that the duty cycle allows for the transmitter to be on for only short periods of time which saves on transmission power and on the life of the transmitter.

In pulse Doppler radar, frequency coherent pulses are necessary for Doppler analysis [2]. The use of the same oscillator for both the transmitter and the receiver guarantees the coherence of the return signal. The receiver is usually a superheterodyne receiver whose output is the input of the complex demodulation stage. The complex demodulation of the radar return creates the complex IQ sequence.

"Processor" is a very generalized name for everything else the radar system does. Included in this stage is clutter rejection filtering which is further explained in Section 1.4. Also included are any type of target detection scheme, Doppler analysis (explained in Section 1.3), and the processing necessary to translate the echo signal data into a useful display.

1.1 Pulse Doppler Radar

A large part of radar that operates by the transmission of pulses can be broadly categorized as pulse Doppler radar. Doppler refers to the use of the Doppler principle in processing. Pulse Doppler radar is classified by the frequency of the transmission of pulses or the pulse repetition frequency (PRF), and the ranges of PRF's used are generally described as low, medium, and high. Modern radar systems include the capability to switch the PRF in order to make full use of the radar's advantages.

A low PRF radar transmits a pulse which is intended to travel to and from the target of interest before the next pulse is transmitted. The PRF is normally on the order of 1 to 3 kHz. The range R to the target is a function of the time t it takes for the pulse to return to the receiver such that

$$R = ct/2 \tag{1.1}$$

where c is the speed of light and where the factor of two enters the equation due to the fact that the signal travels the distance between the radar and the target twice.

The maximum unambiguous range R_u is determined by the maximum amount of time between the transmitted pulses, or the interpulse period T, so that

$$R_u = cT/2 \ . \tag{1.2}$$

If the pulse takes longer than T to travel to the target and return to the radar, the range is ambiguous because it would not be clear which transmitted pulse was the cause of which return. With a PRF of 3 kHz, the maximum radar range becomes 50 km. Some do not classify low PRF radar as pulse Doppler radar even though they are similar in operation [1]. Low PRF radar is commonly called a moving target indicator (MTI) and is generally used as long range search radar [3, 4].

High PRF radar utilizes PRF's on the order of 100 to 300 kHz. Since this gives a maximum unambiguous range between 0.5 and 1.5 km, the unambiguous ranging capability of a high PRF radar is limited. However, pulsed radar uses the Doppler principle to calculate the target's range rate or its velocity, and as shown in Section 1.3, a radar with a higher PRF has a wider range of detectable velocities than a radar with a lower PRF. As a result, low PRF radar has ambiguities in calculating target velocity.

Medium PRF radar has a PRF range between the low and high PRF's and combines the range ambiguities of high PRF radar and the velocity ambiguities of low PRF radar. By using the principles of PRF switching, medium PRF radar becomes reasonably accurate in both areas and combines good characteristics of both low and high PRF radar. In the end, medium PRF radar has a flexibility which often makes it the best choice for airborne radar [2, 3].

1.2 The Doppler Principle

The Doppler principle refers to the shift in frequency observed when another object is moving at a different velocity. From relativistic kinematics [5], the Doppler effect for electromagnetic radiation is seen by

$$f_1 = \sqrt{\frac{c-u}{c+u}} f_t \tag{1.3}$$

where c is the speed of light, f_t is the frequency transmitted from the radar source, and f_1 is the frequency observed at a target moving relative to the source with velocity u. The relative velocity u can be interpreted as

$$u = v_i - v_a \tag{1.4}$$

where v_i is the velocity of the target and v_a is the velocity of the source. By recognizing that the speed of light is much greater than the relative target velocity, the relationship becomes

$$f_1 = f_t \left(1 - \frac{v_i - v_a}{c}\right) . \tag{1.5}$$

The receiver picks up f_1 shifted again so that

$$f_r = f_1 \left(1 - \frac{v_i - v_a}{c}\right) = f_t \left(1 - 2\frac{v_i - v_a}{c} + \left[\frac{v_i - v_a}{c}\right]^2\right) \tag{1.6}$$

where f_r is the frequency of the received signal. Since $c >> v_i - v_a$, the squared term becomes negligible and

$$f_r = f_t \left(1 - 2\frac{v_i - v_a}{c}\right) . \tag{1.7}$$

To see the Doppler shift in the frequency domain, take the transmitted pulse

$$s(t) = A\cos(2\pi f_t t) \tag{1.8}$$

where A is the amplitude and the spectrum of $s(t)$ is

$$S(f) = \frac{1}{2}Ae^{j(2\pi f_t t + \phi)} + \frac{1}{2}Ae^{-j(2\pi f_t t + \phi)} \tag{1.9}$$

with phase ϕ. The return spectrum from a point target is

$$S_r(f) = \frac{1}{2}A_r e^{j(2\pi f_r t + \phi_r)} + \frac{1}{2}A_r e^{-j(2\pi f_r t + \phi_r)} \tag{1.10}$$

where f_r is given by (1.7) and A_r and ϕ_r are respectively the amplitude and phase of the return signal. The difference between the returned frequency and the transmitted frequency is

$$f_r - f_t = -2\frac{f_t(v_i - v_a)}{c} \tag{1.11}$$

which is defined as the Doppler shift.

1.3 Doppler Analysis

In conventional radar notation a positive frequency shift indicates an approaching target and a negative shift indicates a receding target as shown in (1.11). In order to keep from having to make the frequency comparison at the transmitted frequency, the return signal is demodulated down to an intermediate frequency such that the frequency shift of a return from a stationary object shows up as a frequency shift of zero. The demodulation of the return signal is accomplished by its multiplication by a single-sided complex exponential whose frequency is dependent on several factors involving the source velocity and the geometry of the radar scanning. The return signal is a discrete sequence of the total return sampled at the PRF rate. The result of the demodulation is a complex sample for each pulse. By passing the complex sequence through a low-pass filter, a complex baseband sequence is created. The resulting complex sequence is called an IQ sequence denoting the fact that the signal can be divided up into its real and imaginary parts, also called the in-phase and quadrature-phase components of the complex signal.

Based on Fourier theory for discrete signals, the maximum velocity discernable with a pulse Doppler radar is limited by the PRF selected. In order to detect a maximum velocity of $\pm V_{max}$, the minimum value of PRF is given by

$$\mathrm{PRF}_{min} = 4V_{max}/\lambda \tag{1.12}$$

where λ is the wavelength of the transmitted signal [1]. Since the frequency shift is best seen in the frequency domain, the Discrete Fourier Transform (DFT) can be used to obtain the frequency spectrum of the return signal. Because the radar signal is the complex IQ sequence, the maximum range of the frequency spectrum is the PRF. Any speeds that are multiples of V_{max} will cause a Doppler shift that will equal zero and thus are called blind speeds. Any speeds that are greater than V_{max} will be aliased, and their true velocities will be ambiguous.

1.4 Clutter

In any detection system an important factor in the probability of detection is the signal-to-noise ratio (SNR). In communication systems noise comes from the channel through which the signal is transmitted and from the system hardware. Since a radar return is a reflection of transmitted energy, extra noise comes from the reflection of energy from undesired objects. Such noise is called clutter.

The definition of clutter returns depends on the application of the radar system. A ground-based system designed to detect aircraft would receive undesirable returns from birds and weather. An airborne radar used to detect other aircraft would consider returns from anything on the ground and any weather as clutter, while an airborne radar for detecting land vehicles would not consider all ground returns as clutter.

For weather radar the measurement of windspeed is dependent on returns from dust particles, rain droplets, and any other small objects which may be blown around by the wind. Since the individual targets or scatterers are small, the target power received is low. For an airborne weather radar with the antenna scanning downward or in the "lookdown" position, the returns from the ground can be much more powerful than the weather target returns. The concern of this study is lookdown weather radar scanning in the direction of aircraft travel.

Because Doppler radar measures the frequency shift due to the relative motion of the reflecting object, the Doppler shift is used to discriminate between moving and stationary objects. As seen in Section 1.3 the ground clutter is expected to be centered around zero Doppler [2, 6, 7]. Any moving target within the unambiguous Doppler capability of the radar will be found displaced from the ground clutter spectrum center.

For weather radar, clutter can have the effect of biasing the velocity estimate of wind. A proven method for estimating windspeed is to use the pulse pair method of estimating the spectral mean of the radar return after filtering out the clutter

[6, 7, 8, 9, 10, 11]. Clutter rejection filtering is important since the pulse pair estimate gives the spectral mean (as shown in Section 4.3.3), and the presence of any clutter will influence the location of that mean.

All radar systems use some type of a clutter rejection filter to enhance target detection. Particularly for weather radar where the weather return spectrum is distributed in the Doppler processing bandwidth, clutter rejection filtering can also attenuate the power of the low level signal return such that the ability to estimate windspeed can be affected. A method of estimating windspeed without filtering has been considered [6]. However, in most cases clutter rejection filtering is successfully used to aid in the estimation of windspeed [7, 11, 12, 13].

Clutter rejection filtering can be accomplished by various methods. The ground clutter spectrum is expected to be centered around zero Doppler. One method of clutter rejection can be accomplished through the implementation of an ideal filter in the Fourier domain by computing the DFT of the return sequence and then simply zeroing out the signal power levels at and near zero Doppler. A method that may be of limited use in airborne radar is clutter map differencing. The principle behind a clutter map is that the ground objects remain in the same place, but the movement of the aircraft may make this method difficult to use.

Another popular clutter rejection method is the use of a bandstop filter which has a narrow notch centered at zero Doppler. The research at NASA in hazardous windshear detection has made effective use of a second order Butterworth filter with a notch width of ± 3 m/s [12]. Even though the filter is of low order, its effectiveness is due to having a transfer function zero at zero frequency.

1.5 Problem Statement

In the implemention of clutter rejection filters, a problem occurs when the clutter main lobe is shifted away from zero Doppler. Commonly used clutter rejection filters are designed to be effective only in the neighborhood of zero Doppler. As discussed

earlier, in the radar processor the radar return signal is demodulated so that zero Doppler represents a non-moving target return along the antenna beam boresight. However, it is possible that the clutter mode can be shifted away from zero after demodulation, especially for near ranges. For example, a strong target which causes a return through an antenna sidelobe might dominate the radar return at radar ranges less than the boresight range to the ground. An apparent relative velocity would be indicated even though the target is not moving. This clutter mode shifting has been observed in flight experiment data, and attempts have been made to compensate for the problem [14]. Investigated in this work is a method to estimate the shift from the processed radar return and to employ a clutter rejection filter centered around that shift. Such a notch without a frequency reflection which could be centered at any desired frequency would necessitate a filter with complex coefficients. This non-symmetric notch filter is then compared to a conventional symmetric notch filter on the basis of its ability to improve clutter rejection.

Chapter 2 explains the process of centering the clutter spectrum by the super-heterodyne principle. Also presented are various complications to the centering of the clutter spectrum and the theory behind the clutter mode shift versus range in look-down radar. Chapter 3 covers the design of filters with complex coefficients which are derived by transforming a filter with real coefficients. Chapter 4 explains the experiments performed using radar data from NASA's windshear detection experiments and presents various methods of calculating the clutter mode shift. Chapter 5 presents the results of testing a complex filtering scheme on the NASA radar data. Chapter 6 makes concluding remarks and suggests possible avenues for further investigation.

CHAPTER 2

CENTERING THE DOPPLER SPECTRUM

The complex return signal, also called the IQ sequence, is the result of the complex demodulation of the signal. The demodulation of the radar return facilitates its Doppler analysis by showing an increase in the transmitted frequency as a positive frequency shift and a decrease in the transmitted frequency as a negative frequency shift. The radar return has a narrow band of energy determined by the Doppler shift around the transmitted frequency or radio frequency (RF). Radar receivers commonly use superheterodyning [1] to get the signal down to an intermediate frequency (IF). The demodulation of the receiver's IF output is accomplished by the multiplication of the return by the complex exponential $e^{j\omega_0}$ where ω_0 is the appropriate frequency for the centering of the Doppler frequency band.

Superheterodyning refers to the use of two distinct amplification and filtering stages before demodulation of the signal to baseband. The radar return signal is at RF and is mixed with a local oscillator signal to create an IF signal. This signal at IF is then complex demodulated resulting in a two sided spectrum which gives the entire Doppler range from $-$PRF/2 to $+$PRF/2.

2.1 Centering the Radar Return

In order to translate a spectrum to zero Doppler, the radar return is multiplied by a complex exponential at the frequency of the center of the spectrum. That way an approaching or a closing target is seen as a positive frequency signal, and a receding or an opening target returns a signal with a negative frequency.

For a stationary radar, a Doppler shift of zero indicates a stationary target, so that the demodulation by mixing f_t with the return centers the stationary returns at zero. However, for a moving radar platform, as is the case with airborne radar,

stationary objects have a relative velocity with respect to the radar. In order to center at zero the returns from stationary objects such as ground clutter, the demodulation frequency is dependent on the velocity of the aircraft.

Extending the discussion in Section 1.2, for stationary ground clutter the target velocity v_i in (1.4) is zero so that the received frequency of stationary ground clutter in the antenna boresight is given by

$$f_c = f_t(1 + 2v_a/c) \tag{2.1}$$

where v_a is the aircraft velocity in the antenna boresight direction. In order for this frequency to be located at zero Doppler, the frequency for the complex demodulation of the radar return becomes

$$f_{demod} = f_t(1 + 2v_a/c) \ . \tag{2.2}$$

Mixing this frequency with the radar return frequency is equivalent to multiplying the return spectrum by the complex exponential

$$e^{-j2\pi f_{demod}t} = e^{-j2\pi f_t(1+2v_a/c)t} \ . \tag{2.3}$$

Using (1.9) from Section 1.2 as the return spectrum, the result of the multiplication by (2.3) becomes

$$S_{IQ}(f) = \frac{1}{2}A_r e^{j(2\pi[f_r - f_{demod}]t + \phi_r)} + \frac{1}{2}A_r e^{-j(2\pi[f_r + f_{demod}]t + \phi_r)} \tag{2.4}$$

or

$$S_{IQ}(f) = \frac{1}{2}A_r e^{j(2\pi[-2f_t v_i/c]t + \phi_r)} + \frac{1}{2}A_r e^{-j(2\pi[2f_r - 2f_t v_i/c]t + \phi_r)} \ . \tag{2.5}$$

By passing $S_{IQ}(f)$ through a low-pass filter, the result is the complex spectrum

$$S_{IQ}(f) = \frac{1}{2}A_r e^{j(2\pi[-2f_t v_i/c]t + \phi_r)} \ . \tag{2.6}$$

If v_i is the velocity of the ground (which is equal to zero), the result of the demodulation has successfully placed the clutter spectrum at zero frequency.

2.2 Geometric Consideration of Airborne Radar

In (1.4), v_a is defined as the velocity of the source. It should be noted that both v_a and v_i need to be colinear in order for (2.2) to properly demodulate the radar return. The measured aircraft velocity is the groundspeed which is the speed of the aircraft parallel to the ground. When the radar is in lookdown mode, the velocity of the aircraft relative to a point on the ground is not the groundspeed.

As can be seen in Figure 2.1, the apparent radial velocity of a point on the ground is equal to $V_r = -V_g \cos\alpha$ where V_g is the aircraft groundspeed and α is the angle between the direction of the aircraft and the line of sight to the point target. The angle α is a function of both the azimuthal angle ψ_0 and the tilt angle of the radar beam. Notice also that α may differ from the boresight angle α_0 due to the antenna beamwidth. For the airborne radar in consideration here, the narrow beamwidth keeps this difference negligible. The clutter mode shift has been observed to be a function of the range to the ground.

The antenna boresight velocity V_B can be seen in Figure 2.1 to be related to the groundspeed V_g by the angle α_0 such that

$$V_B = -V_g \cos\alpha_0 \ . \tag{2.7}$$

The boresight angle α_0 is related to the azimuth angle ψ_0 by the antenna tilt angle ϕ_0 (not shown in Figure 2.1) so that

$$\cos\alpha_0 = \cos\psi_0 \cos\phi_0 \ . \tag{2.8}$$

This equation is used by substituting $-V_B$ for v_a in (2.2) to center the clutter spectrum.

2.3 Clutter Shifts Due to Sidelobe Returns

In order to determine range information, the radar data is time-gated into range cells. During the interpulse period, the echo time delay determines the range to

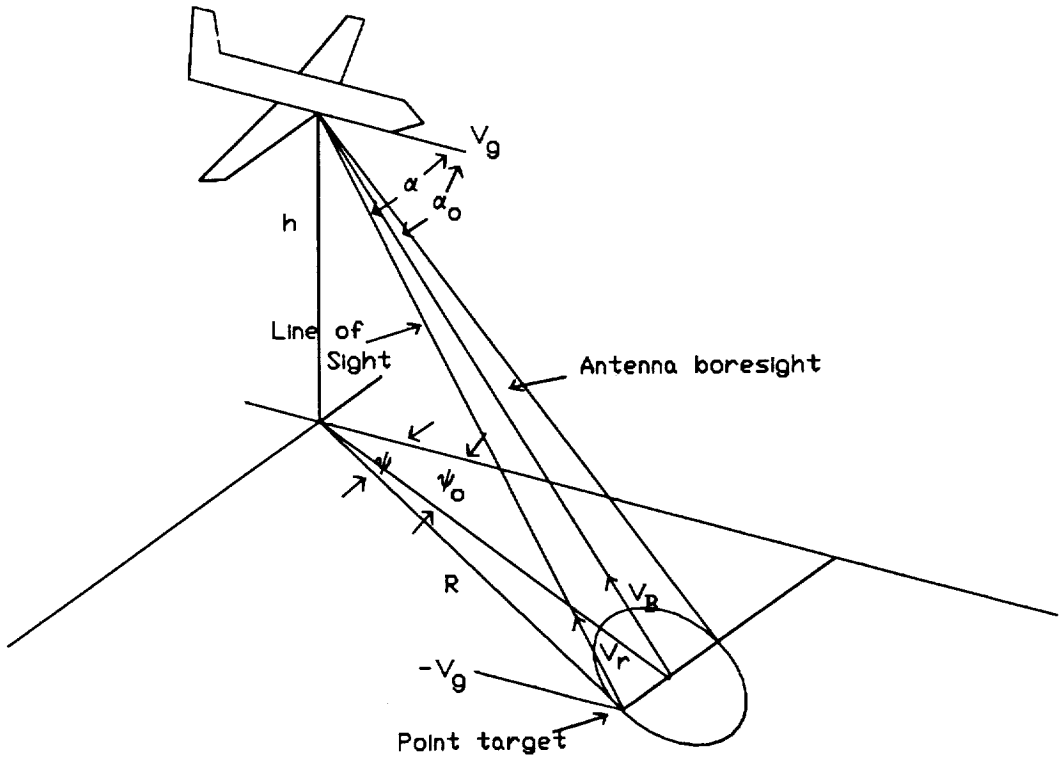

Figure 2.1 Geometry of Lookdown Radar

the reflecting target. In the weather radar situation the target is distributed with many scatterers yielding many echoes. The interpulse period is divided up or gated into range cells each of which can be characterized by a Doppler spectrum. Figure 2.2 shows a graphical representation of the location of radar range cells along the antenna boresight. Portions of the main lobe of the antenna beam will intersect the ground before the boresight does, due to the width of the beam, so that the radar ranges within the main lobe vary considerably from the boresight range. However, in the closest range cells, the antenna main lobe does not intersect the ground at all. The ground clutter returns at slant ranges are from the antenna sidelobes. In the vertical plane, the antenna sidelobes are returned at a different tilt angle than that of the main lobe returns. The tilt angle for the sidelobe returns is dependent on the aircraft altitude and the range to the ground for that particular range cell. The relationship of the sidelobe tilt ϕ_{side} to the range R and the height h is given by

$$\phi_{\text{side}} = \arcsin h/R \ . \tag{2.9}$$

The angle ϕ_{side} can be called the sidelobe angle, because it is the tilt angle at which the sidelobe intersects the ground.

When (2.8) is used in (2.7) to calculate the velocity to be used for the demodulation of the return signal, the boresight velocity V_B becomes

$$V_B = -V_g \cos\psi_0 \cos\phi_0 \tag{2.10}$$

and the demodulating frequency in (2.2) has $v_a = -V_B$. But according to the prediction of the sidelobe influence in the near ranges, (2.10) should be based on the sidelobe angle ϕ_{side} instead of on ϕ_0 so that the radial velocity V_r would be

$$V_r = -V_g \cos\psi_0 \cos(\arcsin h/R) \ . \tag{2.11}$$

Figure 2.3 shows how the cosine of the sidelobe angle differs with the cosine of a constant tilt angle of $-3°$. The difference shown in the figure is $\cos\phi_0 - \cos\phi_{\text{side}}$.

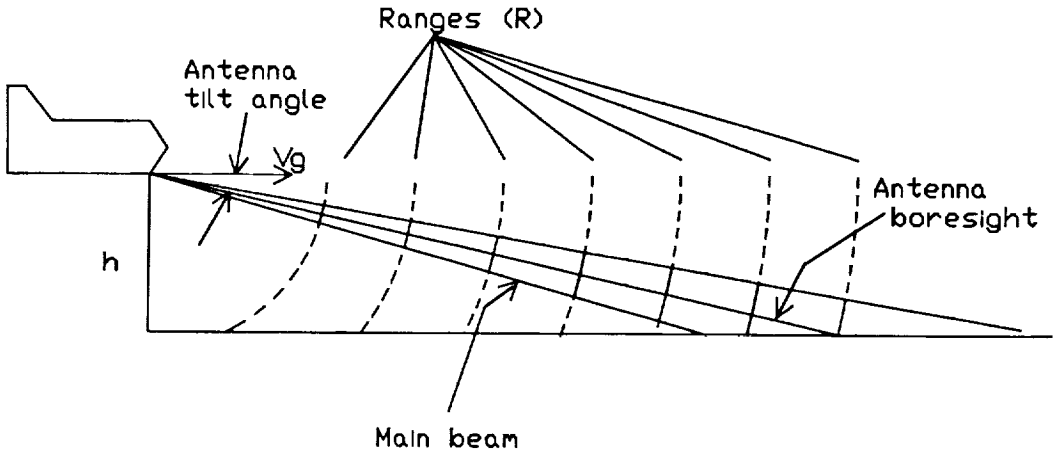

Figure 2.2 Physical Picture of Range Cells

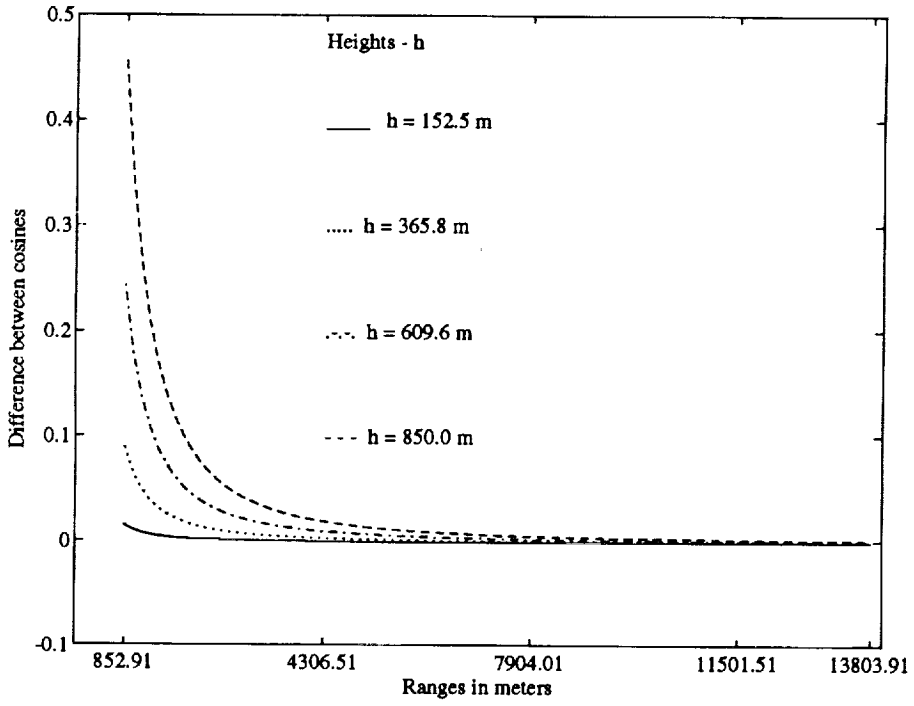

Figure 2.3 Differences Between the Cosines of the Tilt and Sidelobe Angles for Various Heights

Notice that as the range increases, the difference becomes smaller. Also for a lower aircraft altitude the difference is not as great in the close ranges as it is for a higher altitude flight. Of course, for a flight that is of high enough altitude, the near ranges would not even intersect the ground in the sidelobes so that there would be no ground clutter signal for those range cells. However, in low flying aircraft such as in final approach for landing, the possibility of the clutter shift needs to be considered.

2.4 Other Causes of Clutter Shift

Another problem in centering the clutter spectrum is discrete clutter. Discrete clutter consists of returns from unwanted moving objects or large, isolated objects on the ground with a high RCS. In large metropolitan areas a major source of discrete clutter for airborne radar is an airport terminal and the surrounding city and traffic. Discrete clutter from large stationary targets can appear away from zero Doppler and be mistaken for a moving object. The returns from ground traffic and large buildings could possibly be identified by the location of the objects on the ground and from other information based on previous knowledge of the surrounding area and the position of the aircraft. By incorporating this information, an adaptive filter could be used to eliminate clutter from the return signal. The use of adaptive filtering based on modeling the discrete clutter is the subject of continuing research [15].

Another possible cause for the clutter shift is the composition of the ground itself. The amount of power returned in a radar echo depends on the RCS of the scatterer. In the case of the ground, the RCS is represented as a differential RCS which is averaged over a unit area. The effective RCS of the ground changes depending on the moisture of the ground, the amount of vegetation present, and the "flatness" or the shape of the ground. Such factors could have the effect of spreading the clutter spectrum making a mean clutter location less useful. The true effect of the composition of the ground on the clutter spectrum is also a subject of continuing research [31].

2.5 Compensating for Clutter Shifts

In order to remove the effects of clutter on signal detection, the notch filter center frequency should be positioned within the clutter spectrum so that maximum attenuation of the clutter power can occur. Several approaches for the compensation of the effects of clutter mode shifting can be taken. One uses the notch rejection filter centered at zero Doppler. Either the notch width can be adjusted to accommodate for slight variations in the clutter spectrum mode location, or the clutter spectrum can be repositioned to be centered at zero Doppler by demodulating the radar return based on the clutter mode location. Repositioning the clutter spectrum before filtering would necessitate a reshifting of the spectrum back to its original position after the clutter rejection filtering has been accomplished to avoid spectrum aliasing which might bias processing done on the filtered output.

Another method of matching the notch location with the clutter mode location would be to use a notch filter with a movable notch. Such a filter would need to have complex coefficients in order to have a response that is not symmetric about zero Doppler. The design of such a filter is discussed in Chapter 3. The advantage of using a complex filter is that the clutter mode could be filtered without having to shift the clutter spectrum. The main computational requirement is the estimation of the clutter mode location which is also a requirement for the clutter spectrum shifting method. In the analysis to follow the use of a movable notch clutter rejection filter will be considered.

CHAPTER 3

A FILTER WITH COMPLEX COEFFICIENTS

Digital filter design is a basic knowledge necessary in digital signal processing. Radar processors use digital signal processing because it allows sophisticated processing of the radar return signal for automatic detection and tracking. The nature of pulse Doppler radar automatically creates a digital sequence which is the return signal sampled at the PRF. The demodulation of the return creates the IQ sequence which is a complex value for each pulse transmitted. An important part in processing the IQ sequence is the use of digital filters for clutter rejection filtering.

3.1 Digital Filters

One important method of designing digital filters is based on the transformation of an appropriate analog filter. Textbooks discuss the method and theory of designing an analog filter from a prototype and converting it into a digital filter [16, 17]. Signal processing software packages include filter design programs which can be used to design IIR and FIR filters by a number of different methods.

A common factor of these popular filter design methods is that the resulting digital filters all have real coefficients. Of course, real arithmetic is less of a computational load than complex arithmetic. However, a filter with real coefficients is limited to having a frequency response that is symmetric about zero frequency.

Consider the second order Butterworth notch filter with a notch width of $\pm 0.1\pi$. The filter response $\mathcal{H}(z)$ is

$$\mathcal{H}(z) = \frac{0.8006 - 1.6012z^{-1} + 0.8006z^{-2}}{1 - 1.5610z^{-1} + 0.6414z^{-2}}\,, \tag{3.1}$$

and the magnitude of the response is shown in Figure 3.1. The filter in (3.1) will attenuate by more than 3 dB any signal whose frequency is less than 0.1π. In order

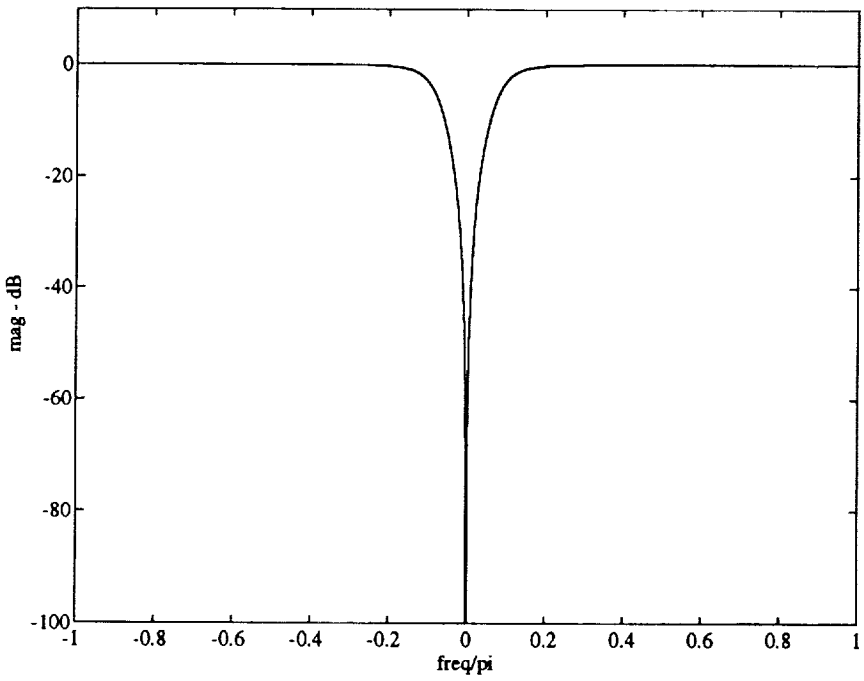

Figure 3.1 Real Filter with Notch at Zero

to attenuate by at least 3 dB a signal at 0.3π, either the notch could be widened, which would filter out every signal less than 0.3π, or the notch could be moved. Redesigning a Butterworth filter with an equivalent notch located at 0.3π while retaining real coefficients results in the transfer function

$$\mathcal{H}_t(z) = \frac{0.6389 - 1.5105z^{-1} + 2.1706z^{-2} - 1.5105z^{-3} + 0.6389z^{-4}}{1 - 1.8575z^{-1} + 2.0357z^{-2} - 1.1635z^{-3} + 0.4128z^{-4}} \ . \tag{3.2}$$

The filter has now become a fourth order filter, and as seen in the magnitude of the response of $\mathcal{H}_t(z)$ in Figure 3.2, the filter not only stops a signal at 0.3π but also any signal at -0.3π. The only way to have a notch filter which would attenuate a positive frequency without any attenuation at the negative of that frequency is to design a filter with complex coefficients.

3.2 A Filter with a Shifted Frequency Response

Because conventional filter design theory cannot directly solve for complex filter coefficients, the complex filter is derived by the transformation of a real filter. A simple transformation is a frequency shifting transformation which centers the frequency response away from zero [18]. The frequency shifting transformation is based on the representation of a bandpass signal as a low-pass envelope times a complex exponential. For the bandpass signal $z(t)$ centered at ω_c, its envelope $x(t)$ is multiplied by $\exp[j\omega_c t]$ so that

$$z(t) = x(t)e^{j\omega_c t} \ . \tag{3.3}$$

By taking the Fourier transform of $z(t)$, the bandpass signal becomes

$$Z(\omega) = X(\omega - \omega_c) \tag{3.4}$$

which is the envelope signal shifted to the frequency ω_c.

Another way to represent a complex signal is to recognize it as a real signal with the negative frequency components zeroed out. The creation of such a signal is accomplished by letting the real part be the original real signal and by having the

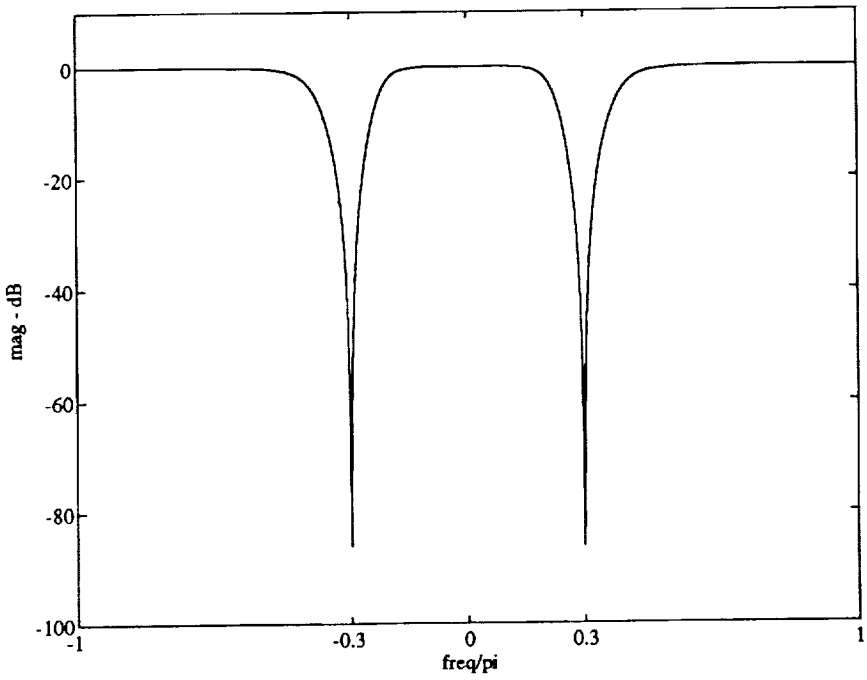

Figure 3.2 Real Filter with Notch Shifted to 0.3π

imaginary part equal the Hilbert transform of the real signal. The Hilbert transform of a real signal $x(t)$ is

$$\hat{x}(t) = x(t) * \frac{1}{\pi t} . \tag{3.5}$$

Basically the transformation results in a $-90°$ phase shift of the original. For example, the signal

$$x(t) = A\cos(\omega_0 t + \phi) \tag{3.6}$$

has the Hilbert transform

$$\hat{x}(t) = A\sin(\omega_0 t + \phi) . \tag{3.7}$$

A complex signal whose imaginary part is the Hilbert transform of its real part is called an analytic signal, and it has half the bandwidth of the original real signal. From the example above, the analytic signal would be

$$x(t) + j\hat{x}(t) = A[\cos(\omega_0 t + \phi) + j\sin(\omega_0 t + \phi)] \tag{3.8}$$

which is equal to the complex exponential $Ae^{j(\omega_0 t+\phi)}$.

To create a complex filter centered at $\omega_c \neq 0$ the filter impulse response is multiplied by $\exp[j\omega_c t]$ as shown above. This equates to replacing s by $s_1 = s - j\omega_c$ in the transfer function $H(s)$ of the filter with real coefficients. Realizing that the s-plane is related to the z-plane by the relationship

$$z = e^{sT} , \tag{3.9}$$

we can determine that z will be replaced by

$$z_1 = e^{s_1 T} = e^{(s-j\omega_c)T} = e^{-j\omega_c T} z \tag{3.10}$$

in $\mathcal{H}(z)$. By letting

$$\gamma = e^{-j\omega_c T} , \tag{3.11}$$

we see that (3.10) becomes z replaced by $z_1 = \gamma z$.

Since each pole or zero is described by

$$(z - a) = 0 \ , \tag{3.12}$$

it follows that replacing z with z_1 results in the pole or zero becoming

$$(z - \gamma^{-1}a) = 0 \ . \tag{3.13}$$

In other words the shifted pole is the original pole rotated by $\omega_c T$ radians. The filter response can be written as the ratio of polynomials

$$\mathcal{H}(z) = \frac{a_0 + a_1 z + \cdots + a_n z^n}{b_0 + b_1 z + \cdots + b_m z^m} \ , \tag{3.14}$$

and the shifted filter becomes

$$\mathcal{H}_s(z) = \frac{a_{0s} + a_{1s} z + \cdots + a_{ns} z^n}{b_{0s} + b_{1s} z + \cdots + b_{ms} z^m} \tag{3.15}$$

where a_{ls} and b_{ls} are the complex coefficients and are derived by

$$a_{ls} = \gamma^l a_l \quad \text{and} \quad b_{ls} = \gamma^l b_l. \tag{3.16}$$

For a transfer function in terms of polynomials in the delay operator z^{-1}, the complex coefficients become

$$c_{ls} = \gamma^{-l} c_l \quad \text{and} \quad d_{ls} = \gamma^{-l} d_l \ , \tag{3.17}$$

and

$$\mathcal{H}_s(z) = \frac{c_{0s} + c_{1s} z^{-1} + \cdots + c_{ns} z^{-n}}{d_{0s} + d_{1s} z^{-1} + \cdots + d_{ms} z^{-m}} \ . \tag{3.18}$$

To see an example of this transformation, note the filter response in (3.1) with a shift to 0.3π. Using (3.10) the filter response becomes

$$\mathcal{H}_c(z) = \frac{0.8006 - (0.9412 + j1.2954)z^{-1} - (0.2474 - j0.7614)z^{-2}}{1 - (0.9175 + j1.2629)z^{-1} - (0.1982 - j0.6100)z^{-2}} \ , \tag{3.19}$$

and the magnitude response does not have the negative frequency reflection as shown in Figure 3.3. Also notice that the order of the filter is preserved.

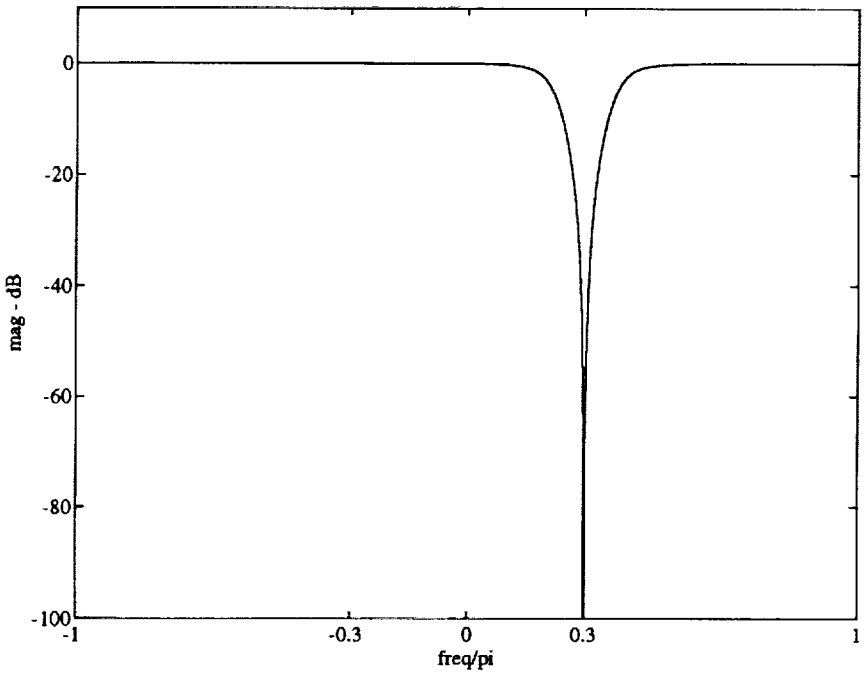

Figure 3.3 Complex Filter with Notch at 0.3π

3.3 A Filter with an Asymmetric Frequency Response

Another transformation which shifts the center frequency of the filter response has been described in the literature [19], but it yields a magnitude response which is asymmetrical about the center frequency. This transformation is accomplished by using the bilinear complex function

$$s = \frac{s_1 - j\alpha}{1 + j\alpha s_1} \tag{3.20}$$

as a frequency transformation function. The most general form of the transformation is given by

$$s = \frac{(ms_1 - jx) - j\alpha}{1 + j\alpha(ms_1 - jx)} \tag{3.21}$$

where the parameters m, x, and $\alpha(|\alpha| < 1)$ are parameters that determine the bandwidth, the center frequency, and the asymmetrical characteristic of the desired complex filter. By using the bilinear transformation to change analog to digital, the filter transformation becomes

$$z^{-1} = \frac{b^*}{b}\frac{a^* + z_1^{-1}}{1 + az_1^{-1}} \tag{3.22}$$

where

$$a = \frac{1 + \alpha x - m - j(\alpha m + x + \alpha)}{1 + \alpha x + m + j(\alpha m - x - \alpha)} \tag{3.23}$$

and

$$b = 1 + \alpha x + m + j(\alpha m - x - \alpha)\ . \tag{3.24}$$

The parameters m, x, and α are solved for by equations involving the desired shape of the resultant filter [19].

To see how this transformation works, consider again the filter of (3.1). Assuming the parameters $m = 0.6283$, $x = 0.9425$, and $\alpha = 0.5$, and using (3.22), (3.23) and (3.24), the filter response $\mathcal{H}_a(z)$ becomes the complex transfer function

$$\mathcal{H}_a(z) = \frac{(2.0214 + j1.2809) + (-2.6412 + j3.9913)z^{-1} + (-1.9692 - j1.3597)z^{-2}}{(2.1617 + j1.1603) + (-2.4947 + j0.9039)z^{-1} + (-2.0115 - 1.1842)z^{-2}}\ . \tag{3.25}$$

The asymmetrical response can be seen in Figure 3.4. This transformation is a bit more involved than the frequency shifting transformation, yet it allows for the flexibility of a filter whose response is truly asymmetrical. Other asymmetrical transformations can be created by variations on the original transformation such as the reciprocal of (3.20).

3.4 Implementing the Complex Filter

When a filter with real coefficients is used on a complex or analytic signal, every operation is performed twice. Each delay, addition, and multiplication needs to occur for both the real and the imaginary parts of each complex sample. For each sample the real and imaginary parts need to be kept separate.

For a filter with complex coefficients, the delays and adders remain the same as above. The only difference is in multiplication because of the multiplication of two complex numbers. The multiplication of the complex sample $X(n) = x_r(n) + jx_i(n)$ by the complex coefficient $A = a_r + ja_i$ becomes

$$AX(n) = [a_r r(n) - a_i x(n)] + j[a_i r(n) + a_r x(n)] \; . \tag{3.26}$$

The increase in the number of operations to be performed is the price that is paid for having to use complex arithmetic.

Since complex arithmetic is easily expressed in terms of real arithmetic, real hardware can be used to implement a complex filter [20]. Figure 3.5 shows the real hardware implementation of a complex multiplication. For the other operations, the delays and additions of the real and imaginary parts are done in parallel.

Once the complex components have been established, the complex filter is implemented in the same manner as a real filter. Any of the real filter realizations can be applied to a complex filter, allowing for the realization of the filter in the most desirable configuration. A parallel realization of the complex sections of a filter has a number of good properties since it is a minimum norm structure [20]. A minimum

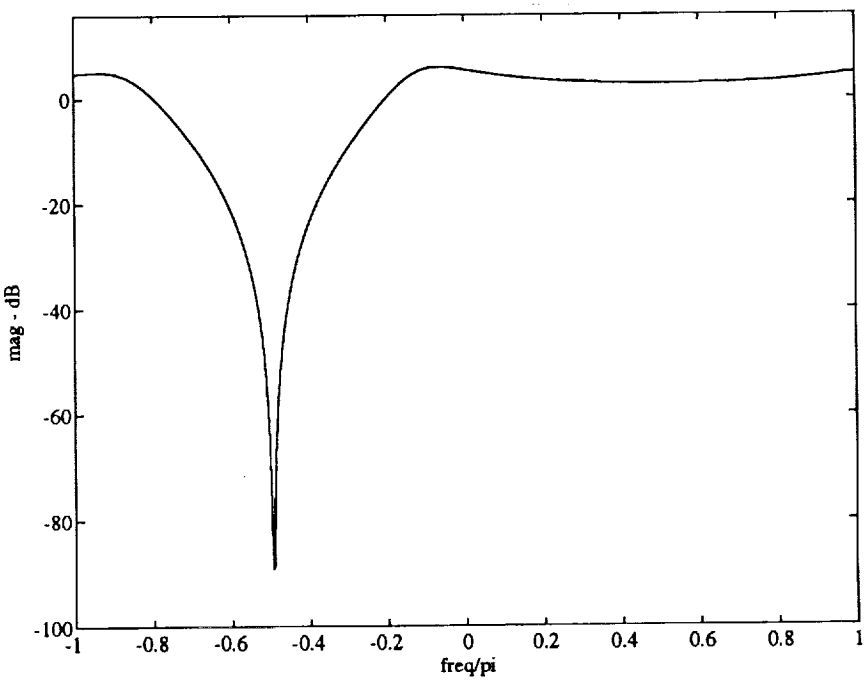

Figure 3.4 Asymetrical Complex Filter

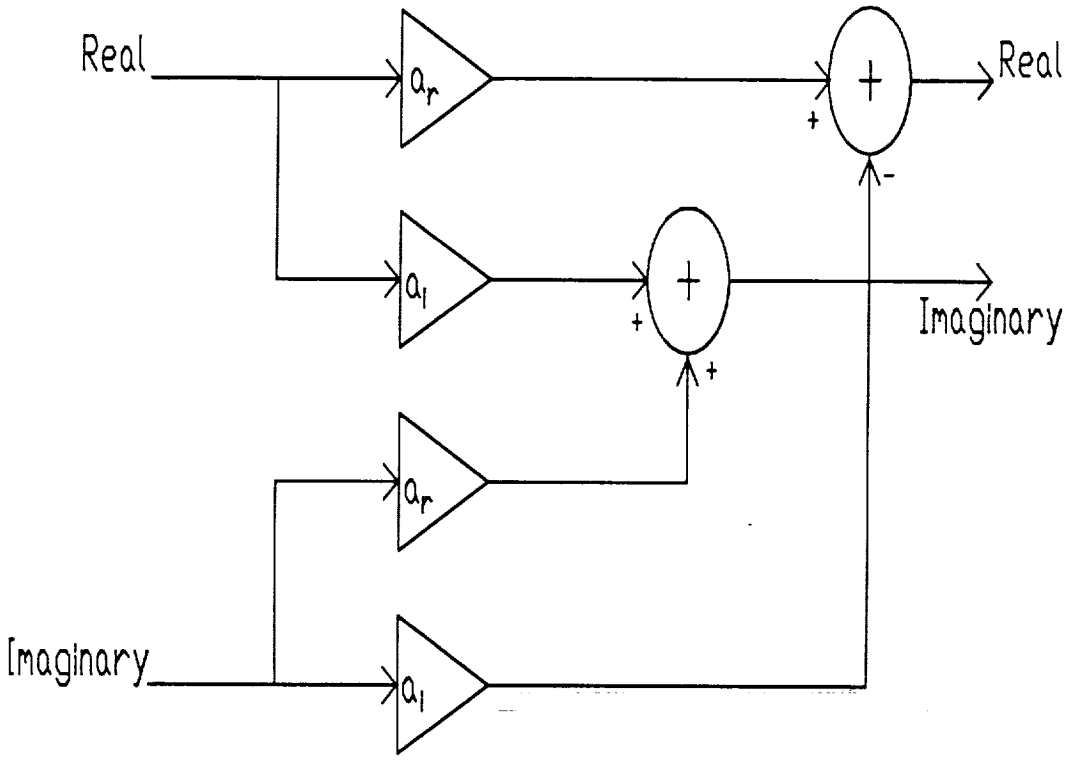

Figure 3.5 Real Hardware Implementation of Complex Multiplication

norm structure is a filter in which the norm of its system matrix has been minimized. In the analysis presented in Chapter 5, the filters are implemented as transposed direct-form II.

It is interesting to notice how shifting the center frequency of the filter affects the notch depth. The original Butterworth filter of (3.1) has a magnitude response of zero at zero frequency. Theoretically, the frequency shifted complex coefficient filter as designed by using (3.10) should also have a magnitude response of zero at the notch location. It turns out that due to coefficient quantization there is a small difference between the actual magnitude response and zero. A filter realized such that it is a minimum norm structure has been shown to have the characteristic of low roundoff noise [21] which could decrease the difference between the actual magnitude response and the desired response of zero. However, the difference is already minute enough that it can be considered to be zero. The ability of the complex coefficient filter to zero out clutter power at the notch location is a desirable characteristic for clutter rejection filtering.

CHAPTER 4

TESTING A MOVABLE NOTCH FILTER

It is quite obvious that a filter with a movable notch could be used to compensate for clutter mode shifts that may occur with airborne radar. To test the use of the movable notch filter, actual radar data are used. The radar data comes from NASA's research in evaluating airborne radar as a means of detecting hazardous weather [13] and is from a forward looking radar operating at low altitudes with a tilt angle of -1 to -3 degrees. Four different approaches are considered for adapting the clutter notch position.

4.1 NASA Research on Hazardous Windshear Detection

Low altitude windshear has been recognized as a potential hazard for aircraft taking off for a flight or approaching for a landing [22]. Since the low-level microburst has been identified as the cause for many plane crashes in the terminal area, NASA has taken up a study on remotely sensing the hazardous weather. The detection of hazardous windshear with airborne pulse Doppler radar has been the topic of many previous papers [6, 7, 10, 11], and the development of a working low-level windshear alert system is now being accomplished at private avionics companies, e. g. [23].

An important part of detecting a hazardous windshear is the definition of what is meant by hazardous. This has led to a definition of the hazard factor based on the horizontal and vertical windspeeds and on the aircraft velocity [24]. Using aircraft accelerometer data to estimate this hazard factor, a severe windshear can be identified with high probability [25]. Although the timing of such an *in situ* identification may not be sufficient for the avoidance of potential catastrophe, such information is useful in the validation of a remotely sensing system.

The investigation into remotely sensing systems has led to several possibilities. Currently in use are the next generation weather radar (NEXRAD) [26] and the

ground based Terminal Doppler Weather Radar (TDWR) [27, 28]. NEXRAD installations form the backbone of the U.S. aviation weather system [29] and can provide detection of low-altitude windshear events. TDWR has proven to be an effective method for detecting windshear and has served as a testing ground for hazard algorithms for airborne systems. A telemetry link from the TDWR to the cockpit can provide direct information to the pilot concerning dangerous locations in the terminal area [30].

The possible forward looking airborne sensors include a pulse Doppler radar, LIDAR (Light Detection and Ranging), and FLIR (Forward Looking Infrared Radiometer). Each system's sensing capabilities can be verified by the *in situ* algorithm and corrolated with data from the TDWR. Future operational windshear detecting systems will likely consist of an integrated combination of various systems.

NASA Langley Research Center has conducted flight tests during 1991 and 1992 including flights at the airports of Orlando and Denver during the potential storm season in the summer. Each flight took place in the near terminal area and included landing approaches and take offs [13]. Many clutter-only flights were performed in order to get a good picture of the ground clutter and the discrete clutter experienced in the terminal area. Weather flights were performed when a storm system was sensed and determined safe enough to fly through. By flying through a storm, the crew could determine the effectiveness of a remote sensing system to estimate the hazard factor as compared to the *in situ* measurements.

4.2 The Radar Data

The radar data used for this paper come from NASA's Wind Shear Flight Experiments. The airborne radar used in these experiments as a remote sensor for hazardous windshear operates in X-band at 9.3 GHz. The radar system can operate at several user-selected PRF's with much of the data collected using a PRF of 3755 Hz with a pulse width of 0.96 μs. The Doppler range at this PRF is ± 30 m/s with a resolution

of 1 m/s. Data were recorded over a range of 14 km to be able to give an advance warning of about 15 to 40 seconds [12]. The azimuth scan of up to $\pm 30°$ guarantees that the entire area in the flight path can be scanned for a possible hazard.

The data used in this analysis consist of records of complex samples from 96 consecutive pulse returns collated according to the radar range. The radar ranges vary from 850 m to 13.8 km including range cells 6 to 96 with each range cell corresponding to the range resolution of the radar, 144 m. Each record of data is indexed according to the antenna scan azimuth angle which varies in 0.5 degree increments over the scan. The data are samples of the receiver IF output and include an AGC (automatic gain control) value within each range cell to extend the effective dynamic range of the A/D converter. The data are "raw" in that there is no pre-processing performed on it.

4.3 Implementing the Movable Notch Filter

The complex filter design method considered here and implemented is the method explained in Section 3.2 and defined by (3.10). The real valued filter which has been most often used in analysis work at NASA is a second order Butterworth high–pass filter with a notch width of ± 3 m/s or $\pm 0.1\pi$. It is readily apparent that shifting the filter notch is a very simple procedure. The main problem is defining where to shift the filter notch.

4.3.1 Predicting the Clutter Mode Shift

For the NASA windshear radar the centering velocity used is given in (2.10). The difference due to the sidelobe angle can be calculated using the altitude information of the aircraft and the range distance of the particular range bin. From (2.11) we get the true radial velocity of the clutter scatterer so that the received frequency of the clutter is given by (1.7) to be

$$f_r = f_t \left[1 + \frac{2V_g}{c} \cos\psi_0 \cos(\arcsin h/R) \right] . \tag{4.1}$$

Since the frequency used in (2.2) uses the boresight velocity of (2.10) the demodulating frequency becomes

$$f_{demod} = f_t \left[1 + \frac{2V_g}{c} \cos\psi_0 \cos\phi_0\right] . \tag{4.2}$$

In the frequency mixing of (2.4) the resulting observed Doppler shift becomes

$$f_r - f_{demod} = f_t \frac{2V_g}{c} \cos\psi_0 \left[\cos(\arcsin[h/R]) - \cos\phi_0\right] \tag{4.3}$$

which ought to be the amount of the clutter shift away from zero. By using this algorithm to predict the shift of the clutter away from zero, the complex filter should be centered at the center of the clutter spectrum.

The accuracy of the prediction of the clutter shift is subject to several variables. First of all, in the closer range cells the angle at which the ground is intersected is out of the main lobe of the radar beam. The resulting spectrum is spread in frequency, usually without a main clutter mode. Another possibility is that second time around returns appearing in the main lobe of the antenna may be of significant relative magnitude to bias the returns in the closer range cells. Second time around returns refer to returns which come from beyond the radar's maximum unambiguous range. Studies have indicated that some second time around returns appear in the closer range bins and that they are less of a problem as the antenna tilt angle increases [31]. The accuracy of the shift predictor is also susceptible to variations in the measurements of the aircraft groundspeed and altitude. A very important point to notice is that a clutter mode shift in the close ranges can occur due to factors other than just the sidelobe returns, which would make the prediction of the shift inaccurate.

4.3.2 The Peak Finder

A possible method for estimating the center frequency shift based on the return data is to use a peak finder. The assumption is that the dominant spectral power mode from ground clutter is located in frequency by the spectral peak and that this is the best position for a clutter rejection filter. In order to implement the peak finder,

a radar signal frequency spectrum estimate is used to identify the frequency location with the largest magnitude.

One problem with the peak finder method of calculating the center frequency shift is that it may be biased by very large returns from discrete clutter such as that associated with moving targets. To discriminate against discrete clutter, a system would need either a logic program that dismisses a solitary peak as discrete or a limiting program that only calculates a frequency shift in the closer range cells where the sidelobe shift is predicted to be more prevalent.

4.3.3 The Pulse Pair Estimator

In a clutter–only situation the location of the spectral mean can be calculated using the pulse pair algorithm. The pulse pair method has been proven to be a desirable way to estimate the mean velocity for a weather return [8] and can be expected to give a reliable estimate of the spectral mean whenever a dominant mode is present. If there is nothing but clutter present in the return, a pulse pair mean estimate should be a good indicator of the clutter mode. The pulse pair estimator is a problem for practical use since it is not a good spectral mode location identifier if more than one mode is present. A discussion of the pulse pair algorithm has appeared in many works on the detection of hazardous windshear [6, 7, 11, 12].

The pulse pair estimate of the spectral mean uses the autocorrelation function estimate of the complex data sequence at the first lag. For a complex sequence x with N data points, the autocorrelation function estimate at the first lag is

$$\hat{R}(1) = \frac{1}{N} \sum_{j=0}^{N-2} x(j+1)x^*(j) \ . \tag{4.4}$$

The pulse pair mean Doppler velocity estimate follows as

$$v_{pp} = -\frac{\lambda}{4\pi T} \arg[\hat{R}(1)] \tag{4.5}$$

where λ is the radar wavelength and T is the interpulse period or 1/PRF. The pulse pair estimator can also be calculated using a power spectrum estimate of the complex sequence x [8].

4.3.4 Autoregressive Modeling

A more sophisticated method of estimating the spectral mode location is based upon the use of the extended Prony method, which uses a linear modeling of the clutter return. Keel uses the autoregressive (AR) model to model the clutter spectrum and thus to design a clutter rejection filter [11]. Earlier work had suggested that the AR model is a useful tool in modeling the ground clutter returns [32]. In Keel's study, a 10th order AR model was used to estimate the clutter spectrum, and a clutter rejection filter was designed by using the inverse of the AR model as an FIR filter. Although the methods presented by Keel are attractive from a theoretical view, the need for a true clutter–only return to create the model and the computational load of AR modeling present implementation problems.

Kunkel [6] employs a second order AR model in an extended Prony algorithm to identify clutter and weather modes. By using his modal analysis principles, it is possible to identify the clutter mode as the location of the clutter spectrum shift. This implementation is similar to the pulse pair estimate, but it is superior in that it accounts for more than just one mode thus enabling the processor to characterize both the weather location and the clutter location when they both appear. At low return power levels the mode estimates tend to fluctuate randomly near the maximum Doppler shift value. A simple power level threshold can be effective in identifying erroneous large shifts.

By using the Levinson–Durbin algorithm to calculate the second order AR coefficients a_1 and a_2, the extended Prony approach solves the characteristic polynomial

$$\mu^2 + a_1\mu + a_2 \tag{4.6}$$

for the values of μ_1 and μ_2 which determine the frequency estimates. The frequency estimates determine the weather and clutter velocities in a manner similar to the pulse pair velocity described above. The velocities are calculated by

$$v_i = -\frac{\lambda}{4\pi T}\arg(\mu_i)\ . \tag{4.7}$$

Kunkel defines the clutter velocity as the velocity whose absolute value is closer to zero of the two velocities [6]. The Levinson–Durbin algorithm is described in Appendix A.

4.4 Testing the Shift Estimators

By using the various shift estimators to locate a notch to filter the clutter return, the effectiveness of each estimator to calculate the clutter spectral shift can be determined. If the signal used is clutter–only, the resulting signal power after filtering can be examined. The shift estimator which is most effective would reject the most clutter and thus would result in the lowest power after filtering.

Another area in which the shift estimators should be compared is in the amount of computation necessary to implement each estimator. Although the peak finder seems simple enough, a DFT computation is required for each range cell. Even with an efficient FFT algorithm, it is still time consuming. The pulse pair estimator uses an autocorrelation estimate which is much more efficient than the FFT. For low order models the modal analysis methods involve simple correlation estimates from the data and can be efficiently implemented. The mode prediction is not data dependent and is thus the simplest of all computationally.

The next chapter details the results of experiments for this work. First of all the shift estimators are compared in their ability to estimate the clutter mode shift. Then the power levels after filtering are compared to see which estimator is the most effective. More importantly the results are used to evaluate the effectiveness of a movable notch filter with complex coefficients as compared to the more conventional fixed notch filter with real coefficients.

CHAPTER 5

RESULTS

In this chapter the predicted clutter shift (as discussed in Section 4.3.1) will be compared to the data dependent clutter shift estimators presented. A shift in the clutter of the closer range cells can be observed by looking at frequency plots of the clutter run data. The data set used for analysis is clutter–only recorded over Denver, Colorado, on 9 July, 1991. The data consist of 257 frames covering an entire antenna scan from 0 to $-30°$ to $+30°$ and back to 0 at 0.5° increments. This scan was randomly selected and consists of frames 200 to 456. Data at scan angles $+5°$ (Frame 200), $-30°$ (Frame 270), and $-6.5°$ (Frame 320) were chosen to be displayed in this chapter, and Appendix B consists of a complete listing of range cell frequency plots for Frame 270. The tilt angle was a constant $-3°$. The variation in the aircraft height and velocity was small since the frames were taken so close to each other, and it turns out that this variation had little effect on the data.

Each spectral estimate is plotted in the weather radar convention of power versus windspeed. The windspeed is calculated from the original Doppler shift equation given in (1.11). For a target moving toward the radar, the relative velocity u is less than zero so that the Doppler shift f_d is greater than zero. Rewriting (1.11) with $u = v_i - v_a$ and $f_d = f_r - f_t$ yields

$$f_d = -\frac{2uf_t}{c}\ , \tag{5.1}$$

which shows the opposite sign relationship between the velocity and the Doppler shift. In the case of weather radar, the centering algorithm removes the aircraft velocity so that the direction of the wind determines the sign of the relative velocity u, and the Doppler frequency shift is as given above. From (1.12) and the radar parameters, the maximum Doppler velocity is ± 30 m/s.

5.1 Observation of the Shift

By analyzing the Doppler spectral estimates of the radar return, the dominant clutter mode is shifted from zero at the shorter ranges. The upper plots of Figures 5.1, 5.2, and 5.3 illustrate the Doppler spectral estimates for each range cell at one antenna scan angle using returns from 96 pulses. The spectral magnitude is simply the relative magnitude within a range cell and has no meaning across range since the range cell dependent AGC value has not been removed. The 3-D plot of Figure 5.2 can be compared with the data in Appendix B since it is from the same frame of data. All signals below 80 dB have been set equal so that the peaks are easier to see. From these plots it is evident that the majority of the greater clutter peaks are near zero Doppler and that some clutter power exists away from zero. Each figure also includes a point density plot formed by thresholding the spectral values in each range cell and projecting the higher values onto a range/frequency plot — or point density plot. The point density plot maps spectral intensity to the density of points. The point density plots can more clearly show the clutter ridges which are sometimes masked in the 3-D plots.

From Figures 5.1, 5.2, and 5.3 a shifting trend is evident in the clutter peaks at the short ranges. The shift is more easily noticed in the point density plot. It is also notable that the shifting trend is not easily recognized in all frames. One answer to this discrepancy is that the clutter returns at closer ranges are more spread in frequency. In fact, cells 6 through 19 of Frame 270 as shown in Appendix B seem to have no main clutter mode. Figure 5.4 shows this "clutter spread" by lowering the floor of the previous 3-D frequency plot from 80 dB down to 70 dB. The peaks of this area may or may not follow the predicted clutter shift, but even if they do they are not necessarily representative of a clutter spectrum mode. Instead of looking like a unimodal spectrum, the short range returns seem to have more nearly a "white" frequency spectrum.

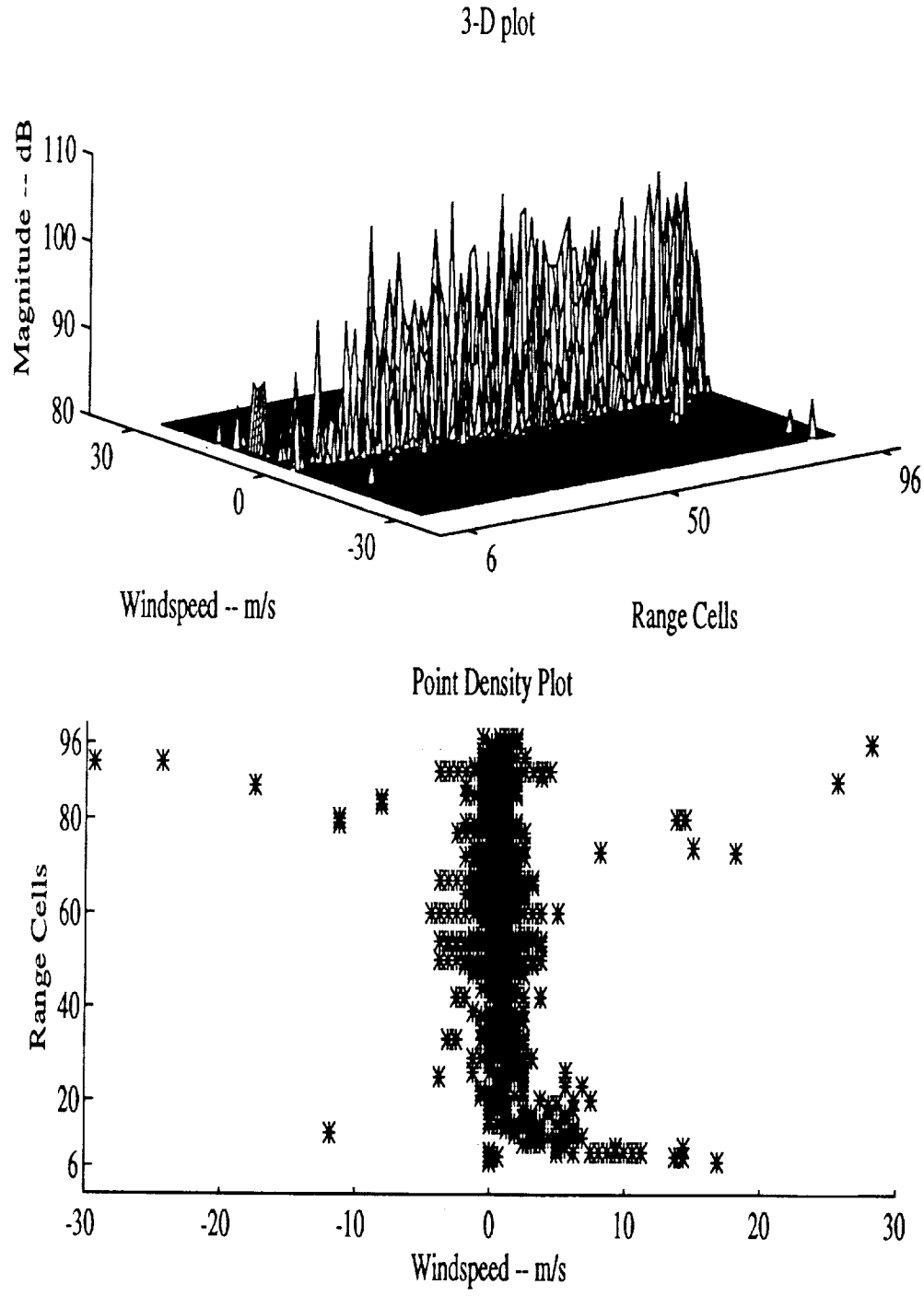

Figure 5.1 Plots of Frame 200

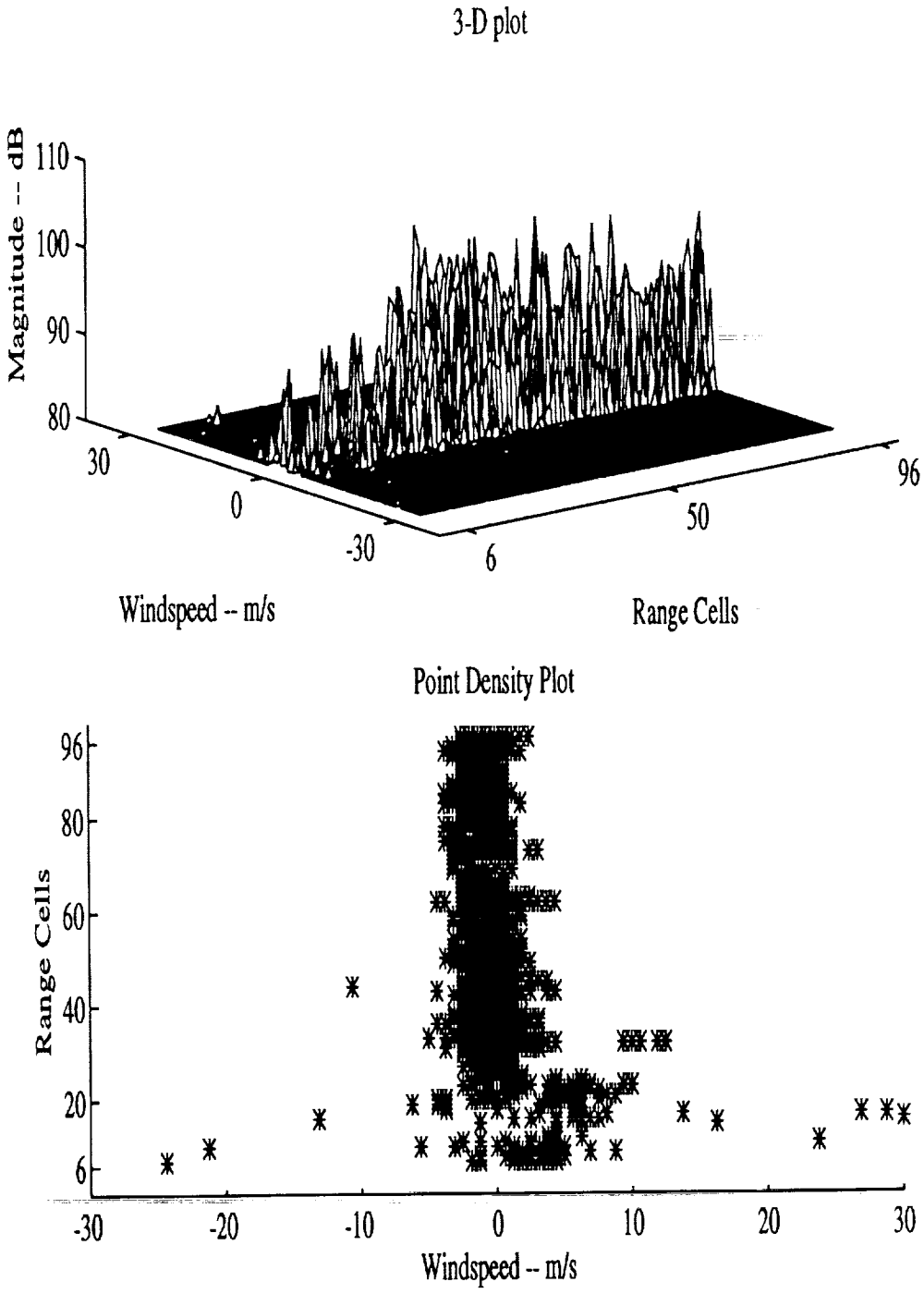

Figure 5.2 Plots of Frame 270

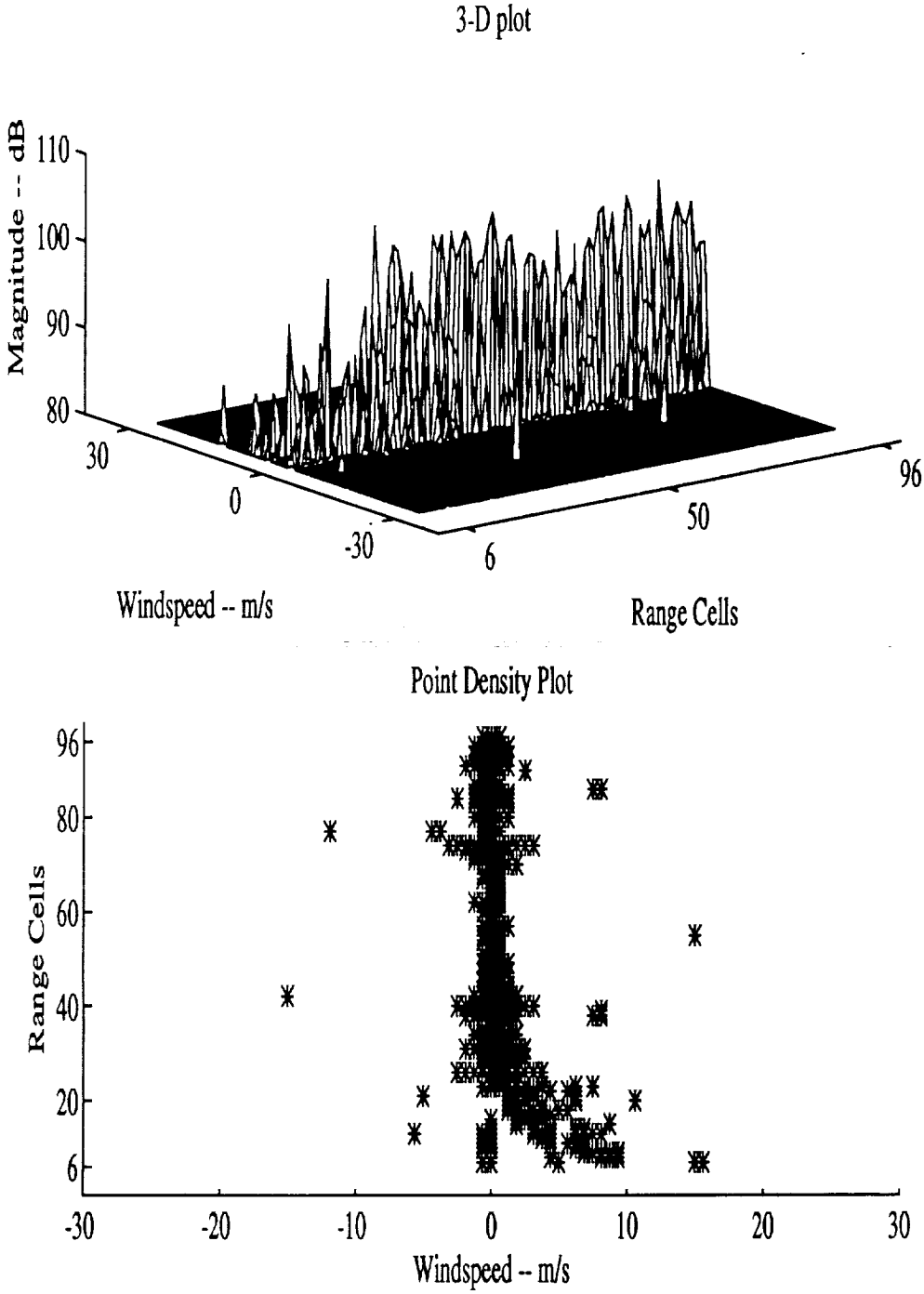

Figure 5.3 Plots of Frame 320

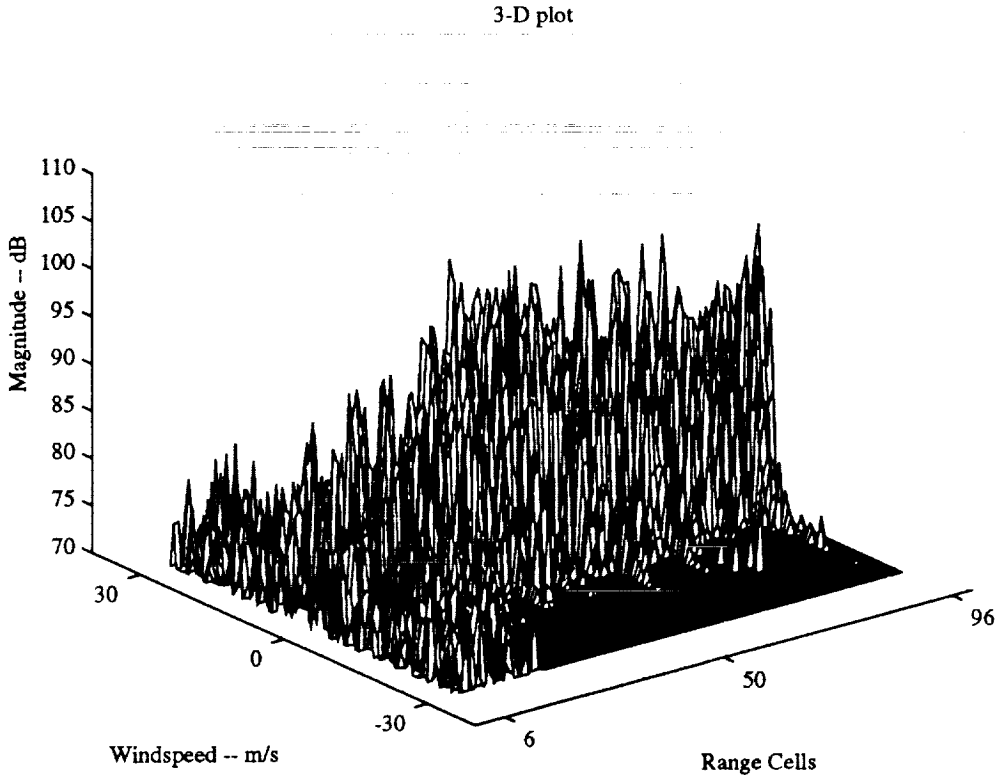

Figure 5.4 Plot of Frame 270 with Floor at 70 dB

5.2 Comparison of the Shift Estimators

As shown in Section 4.3, there exist several methods (the peak finder, the pulse pair estimator, and the extended Prony method) of estimating the frequency shift of the clutter spectrum mode and these estimates can be used to compare the observed clutter mode with the clutter shift predictor given in (4.3). The clutter shift predictor varies with the aircraft height, velocity, and the antenna azimuth angle, and since for this particular flight the height and velocity were relatively constant, the variation depends primarily on the azimuth angle. Even so, the predicted clutter mode shift does not vary significantly for the frames examined.

Figure 5.5 shows the comparison of the peak finder with the frequency shift predictor. The trend of the peak finder does follow the shift predictor, but as can be seen in the comparison on Frame 270, the variance can be large. These variations are mostly due to the Doppler frequency spectral spread and lack of a dominant mode in the close range cell returns as shown in Appendix B. Since the clutter spectra in the closer ranges of Frame 270 are more spread in frequency, characterizing each spectrum as unimodal at a single frequency based on the greatest power may not be useful due to the lack of a dominant clutter mode.

In Figure 5.5 note the peak finder's "spike" in Frame 200 at range cell 82 which may be due to discrete clutter. As mentioned before, discrete clutter can show up as a high energy return away from zero Doppler. Here again, the selection of that peak as the dominant clutter spectral mode is not representative of the true clutter spectrum. By examining the range cell spectra of Frame 270 in Appendix B, the separation of the dominant clutter spectrum and discrete clutter can be easily seen.

Next the pulse pair algorithm as a clutter mean estimator is compared with the frequency shift predictor. In Figure 5.6, the pulse pair estimates of the mean clutter frequency exhibit similar variations as were noted in Figure 5.5 with the peak finder results. Since the pulse pair deviations are not as large as those for the peak finder, one can deduce that there must be more than one spectral "peak" in the cell spectrum

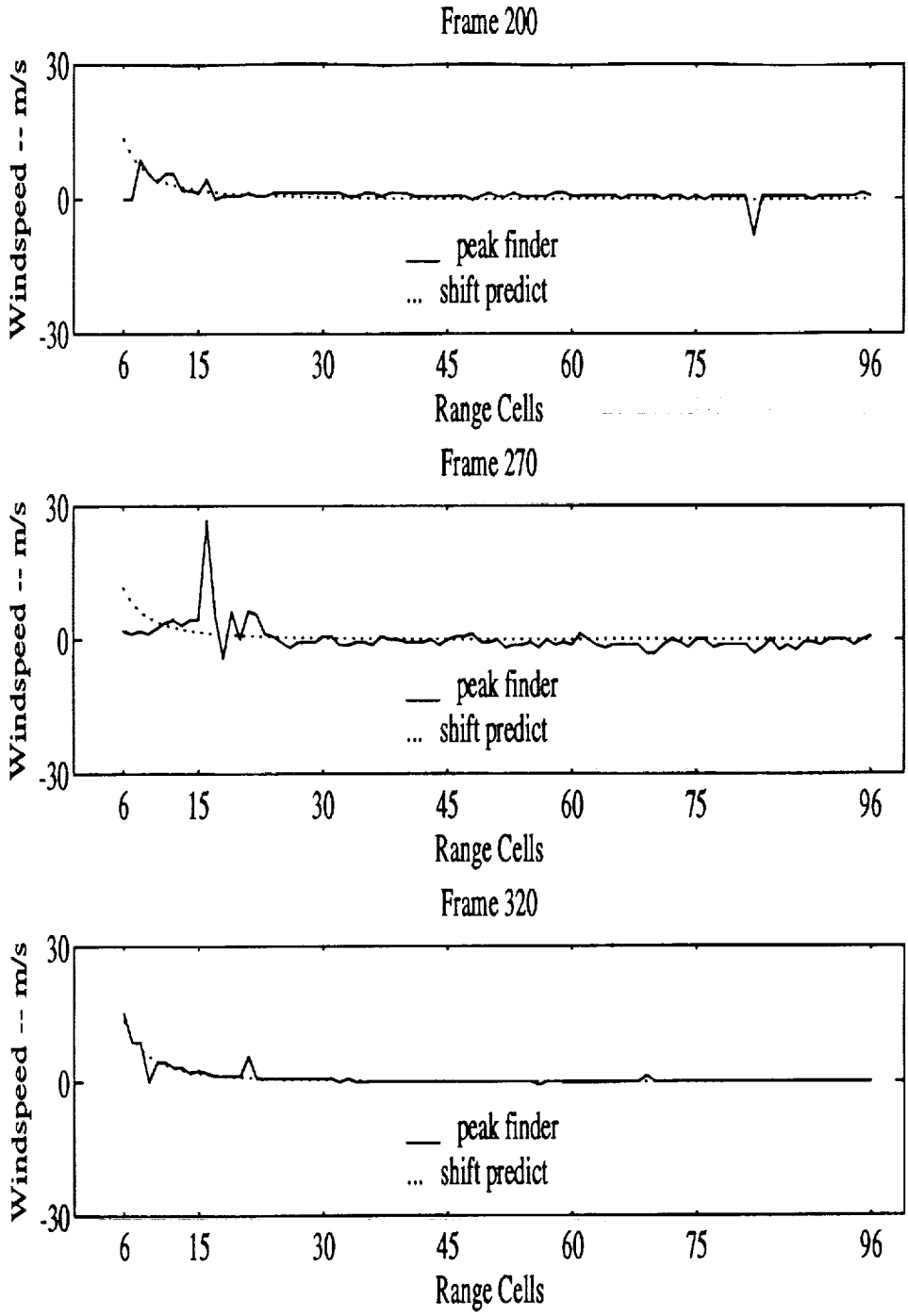

Figure 5.5 Comparison of the Peak Finder with the Shift Predictor

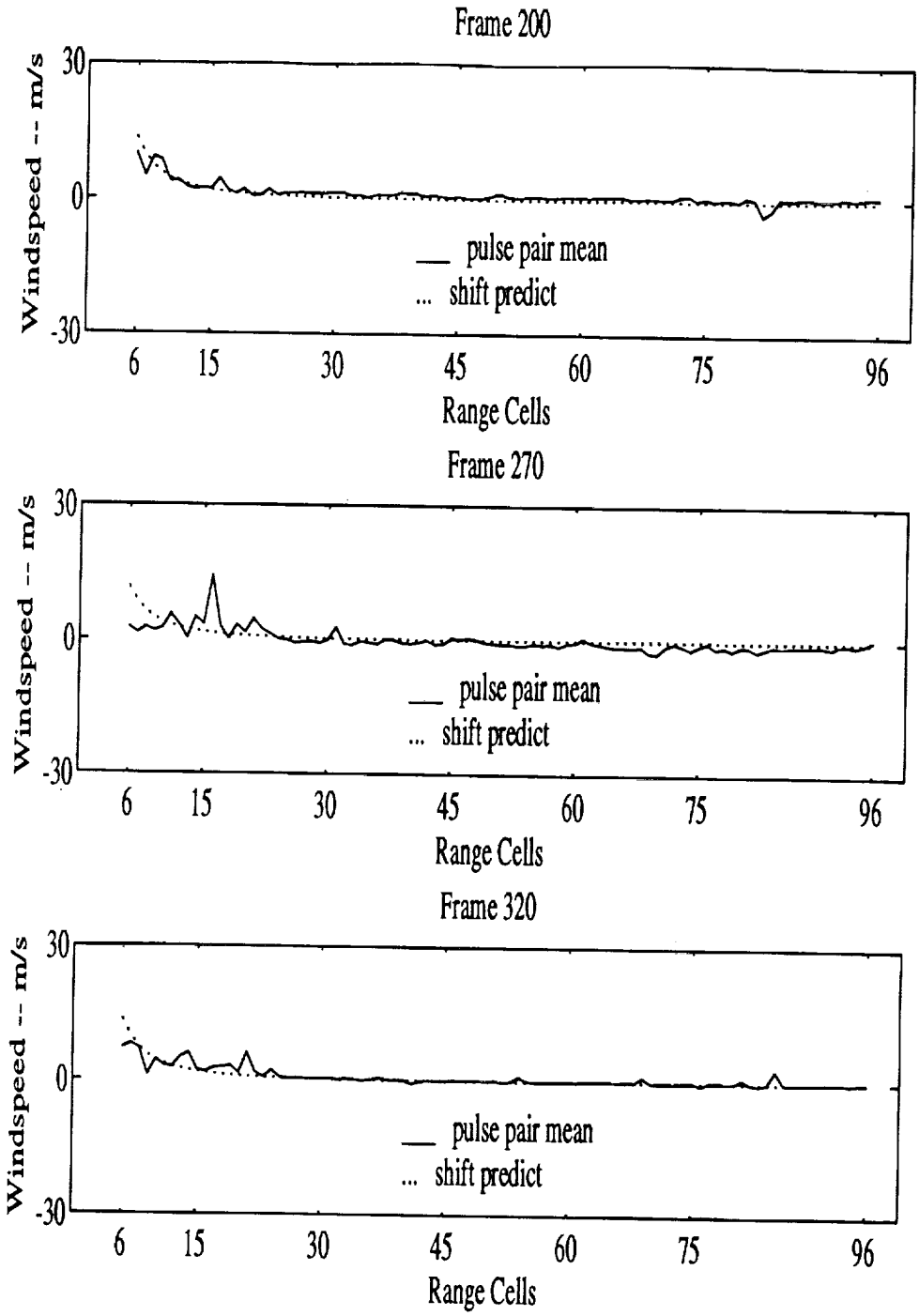

Figure 5.6 Comparison of the Pulse Pair Algorithm with the Shift Predictor

influencing the spectral mean since a single spectral mode would tend to dominate the mean estimate. The multiple peaks can be seen by looking at the spectrum of each range cell as mentioned above.

As it has been shown, the pulse pair algorithm gives a mean over the entire range cell spectrum [6]. Thus a pulse pair estimate for a cell in which discrete clutter is also present would not accurately represent the spectrum of either the dominant clutter near the aircraft groundspeed or the discrete clutter which may be displaced in Doppler. Also in cases where weather returns are present, the pulse pair mean may not accurately estimate the clutter shift. Results using the pulse pair mean are presented here to validate the peak finder.

The extended Prony analysis technique of Section 4.3.4 for estimating the main lobe clutter frequency shift is compared with the frequency shift predictor in Figure 5.7. The extended Prony analysis can also be called the clutter mode identifier since it identifies the "mode" which should represent the clutter spectrum and differentiates it from a weather mode. This second order clutter mode identifier can recognize two distinct modes distinguishing it from the pulse pair algorithm.

As can be seen, the clutter mode technique is similar to the peak finder and the pulse pair algorithm at following the frequency shift predictor. Based on studies involving modal analysis [6], the clutter mode technique probably has the most credibility for providing a good frequency shift estimate. Once again the effect of discrete clutter must be considered. It would appear that the clutter mode technique should be able to identify the main clutter in the presence of a discrete clutter mode although the presence of a weather mode may reduce its effectiveness. A higher order autoregressive model could be used to model the clutter spectrum which in turn could be used to identify not only the main ground clutter location but also any number of discrete clutter locations [11]. Of course the price for a better clutter identifier through a higher order AR model is the increased computational intensity required to solve for the AR coefficients.

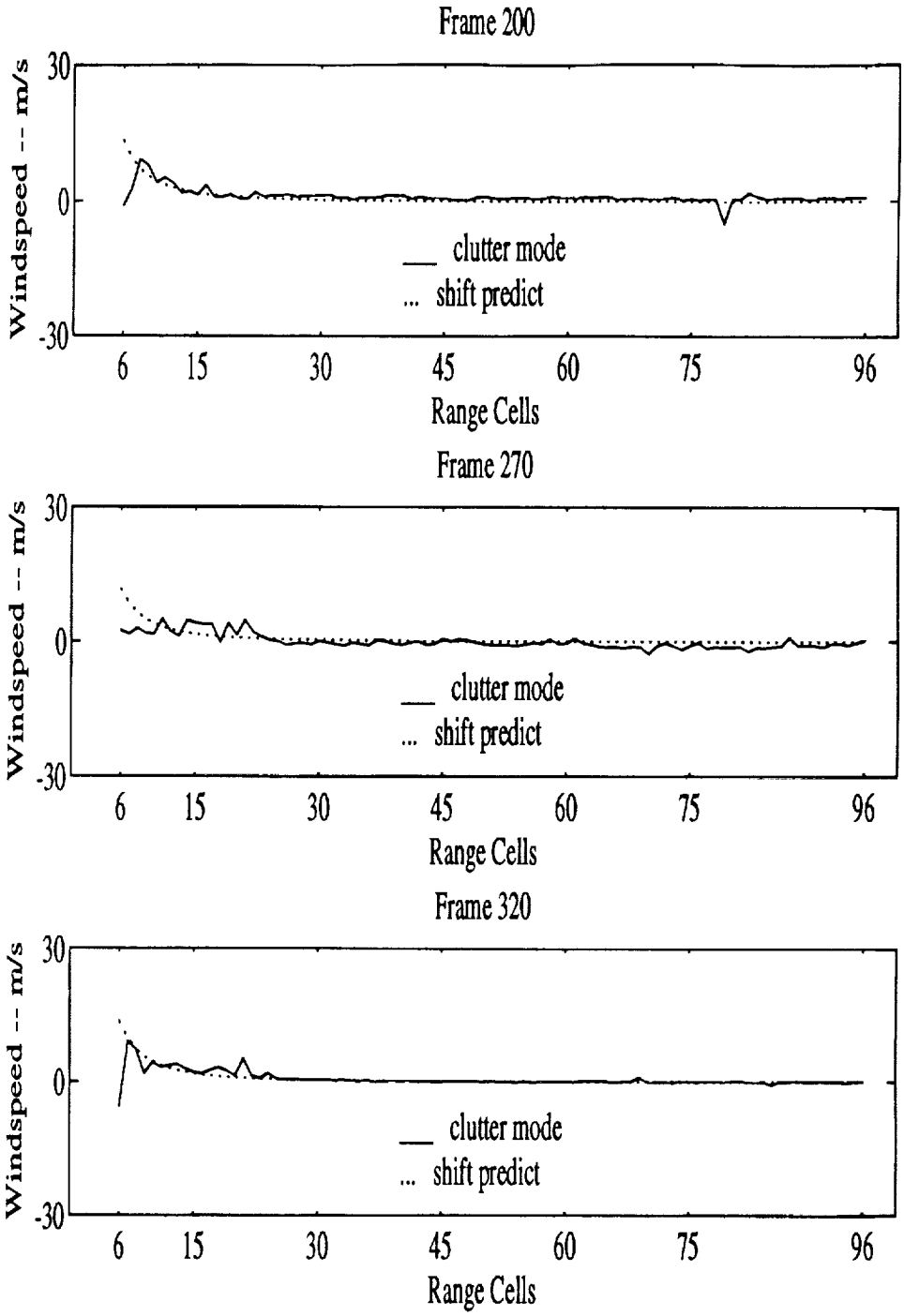

Figure 5.7 Comparison of Clutter Mode Identification with the Shift Predictor

For all the data examined the three shift estimators followed the shift predictor fairly well with a few discrepancies as shown in Frame 270. Based on these results it would seem that any of these shift estimators would be a valid algorithm on which to base the complex notch filter frequency shift.

5.3 Comparison of Complex Filter with Butterworth Filter

Following is an analysis of the performance of a complex filter based on the four frequency shift techniques of Section 4.3 which is compared to the performance of the Butterworth notch filter centered at zero Doppler and currently in use in the NASA radar research. The clutter data from the Denver flight examined was filtered using filters designed by using the various frequency shifting techniques described above. The resulting power is shown for range cells 6 through 30, since most of the frequency shifting occurs in the closer range cells. Figure 5.8 shows the clutter rejection filter gain for the five filtering schemes: the Butterworth notch, the shift predictor centered notch, the pulse pair centered notch, the peak finder centered notch, and the extended Prony centered notch. This gain is the ratio of output power to input power expressed in dB over the entire processing bandwidth. Thus the better the clutter rejection the lower the gain value. Notice that overall the complex filter schemes do better than the Butterworth filter at rejecting clutter. At all the ranges shown except for the closest ranges at range cells 6 and 7, the clutter rejection of each complex filter is greater than or equal to that of the Butterworth filter. Figure 5.9 shows how each complex filter performs relative to the performance of the Butterworth filter. The comparison of the complex filter with the Butterworth filter is made by taking the power out after using the Butterworth clutter rejection filter divided by the power out after filtering with the complex filter. The resulting ratio is called the clutter rejection factor and shows more of an improvement the larger the number. For a factor greater than one the complex filter rejects more clutter power than the Butterworth filter, and for a factor less than one the Butterworth filter rejects more clutter.

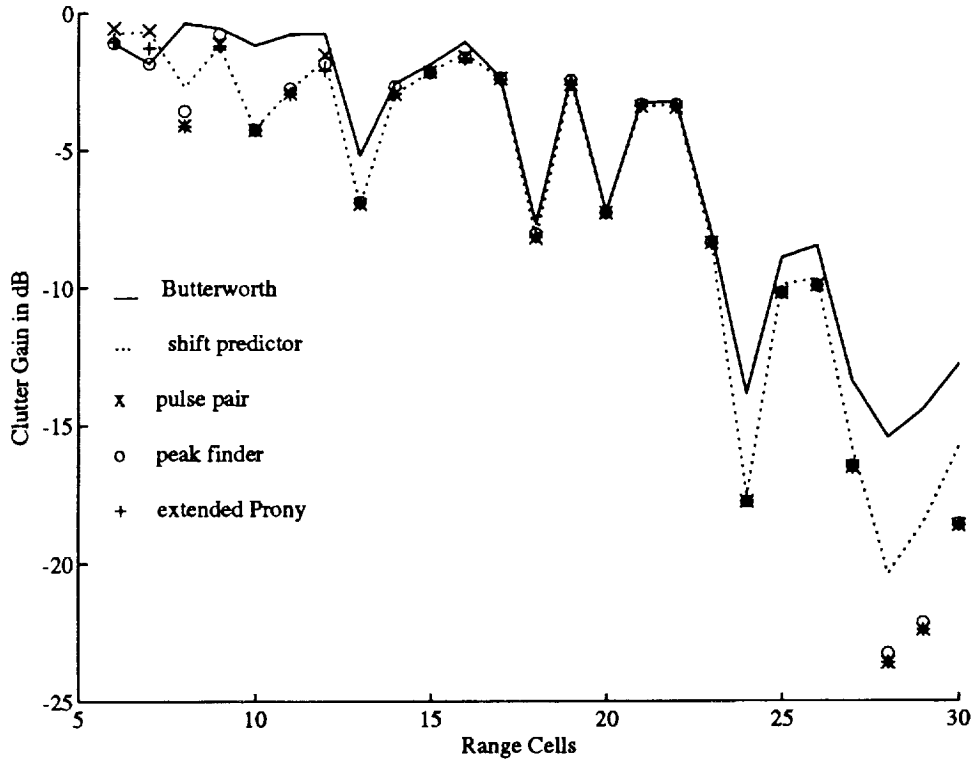

Figure 5.8 Results of Clutter Rejection Filtering for Frame 200

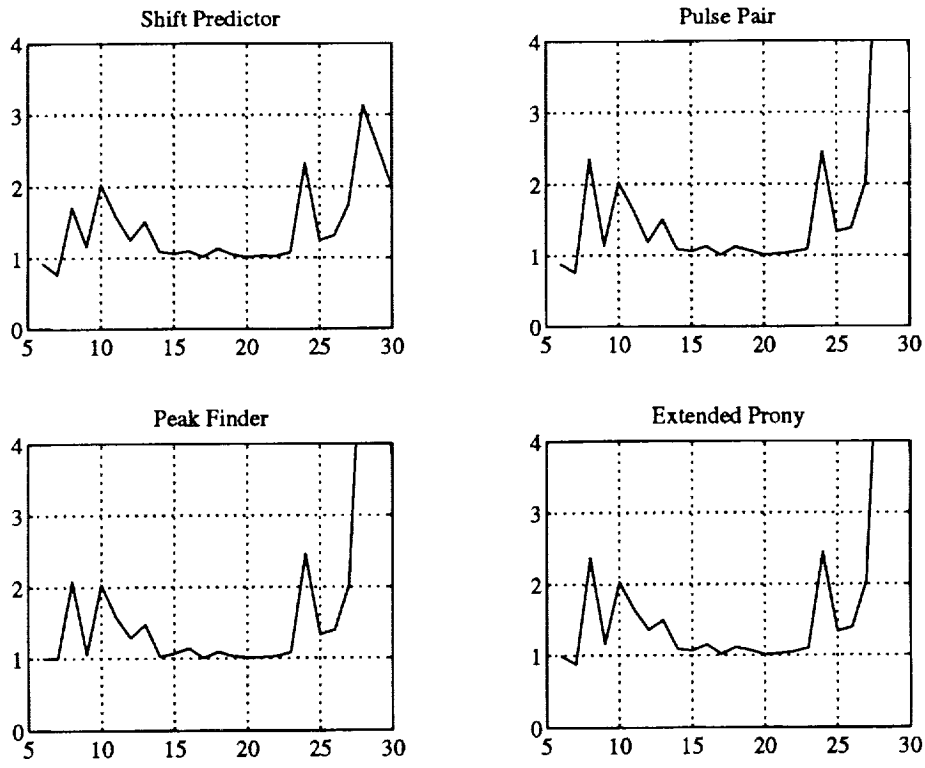

Figure 5.9 Clutter Rejection Factors for Complex Filtering of Frame 200

Figures 5.10 and 5.11 show the clutter gains for Frames 270 and 320 respectively. In each case, all of the filters reject more of the clutter power in returns from longer ranges. In the individual range cell spectra for Frame 270 in Appendix B, the clutter mode can be seen to be more spread at the closer ranges than at ranges that are farther away. When the clutter power becomes more concentrated around a central frequency, all of the clutter rejection filters are able to cancel more of that power. The clutter rejection factors in Figures 5.12 and 5.13 show similar results for Frames 270 and 320. The clutter rejection factors for Frame 270 demonstrate that clutter spectrum spreading at closer ranges reduces the ability to estimate a useful clutter mode shift for the complex filtering routine.

From these results, filtering with a complex filter seems to improve the ability to reject clutter power in the close range cells when a definite clutter mode shift can be identified. The cases in which the complex filter does not improve on the Butterworth filter have a clutter spectrum lacking a dominant mode which can be identified as the major source of clutter power in the return spectrum. In general, the complex filter does a good job of improving clutter rejection.

In terms of the clutter rejection factors, the shift predictor seems to be a poor estimator for the clutter mode shift. As mentioned before, the shift predictor is mainly limited by the theory that sidelobe returns are the only reason for the clutter mode shift in the near ranges. It appears that there is more going on than just sidelobe returns, and the tracking method of the shift estimators seems to be a more robust method for estimating the clutter mode shift than predicting it based on just the aircraft and antenna positions.

As can be observed in the range cell spectra in Appendix B, the closer range cells contain more low level returns that are spread in frequency than the farther range cells. After about range cell 25 the return spectra tend to show more of a dominant mode with the returns at other frequencies decreasing in power. For this reason the

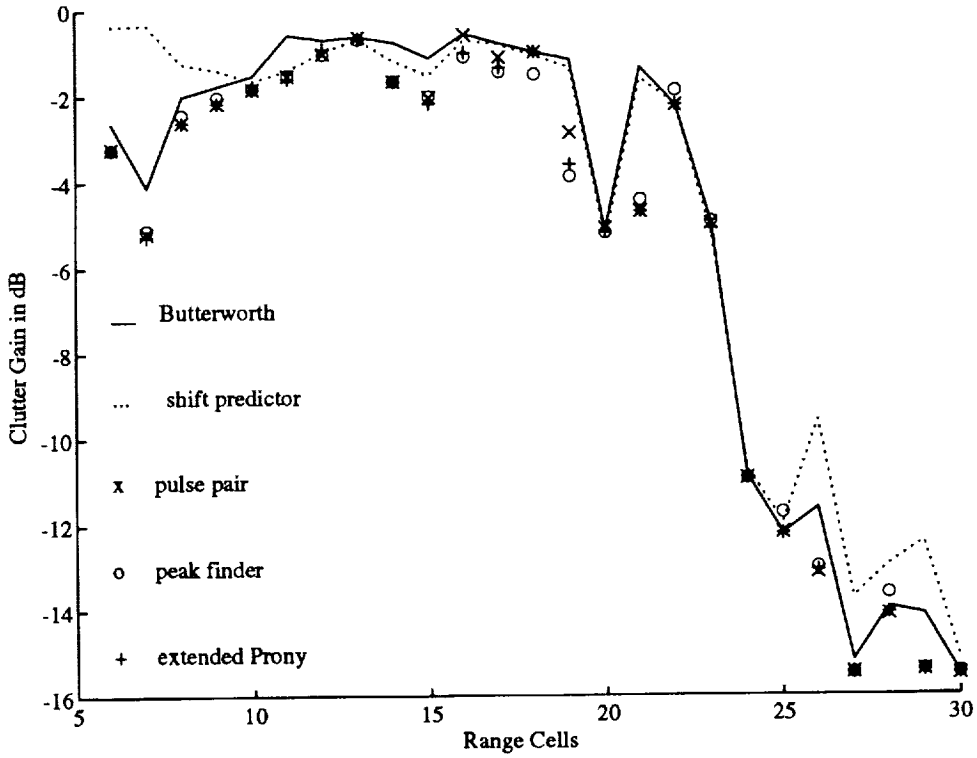

Figure 5.10 Results of Clutter Rejection Filtering for Frame 270

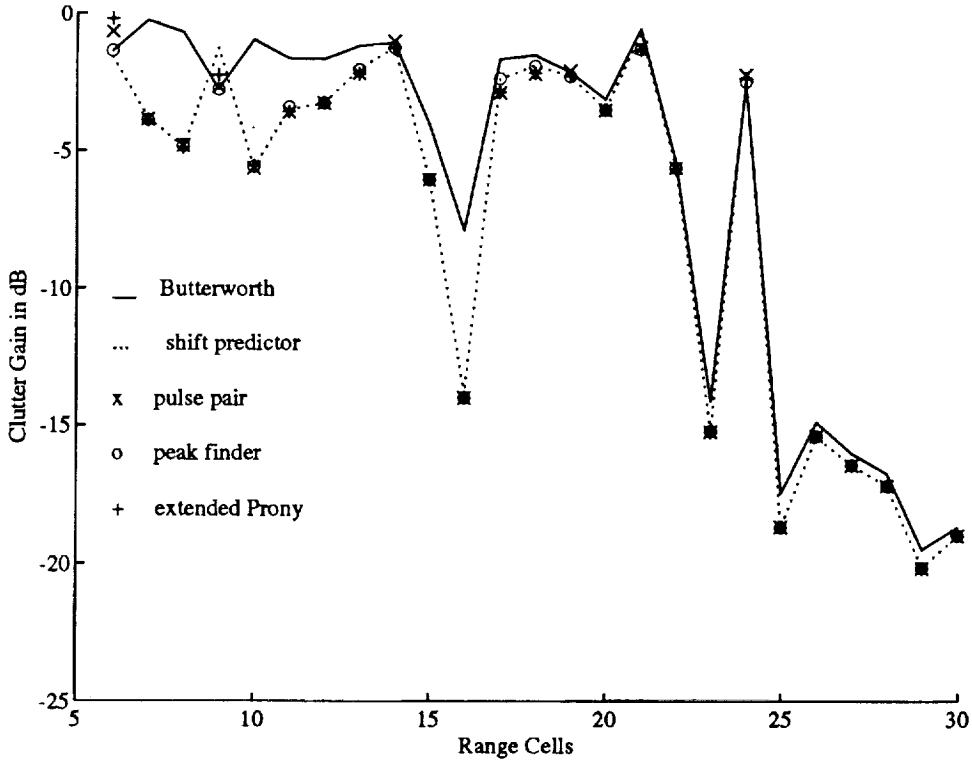

Figure 5.11 Results of Clutter Rejection Filtering for Frame 320

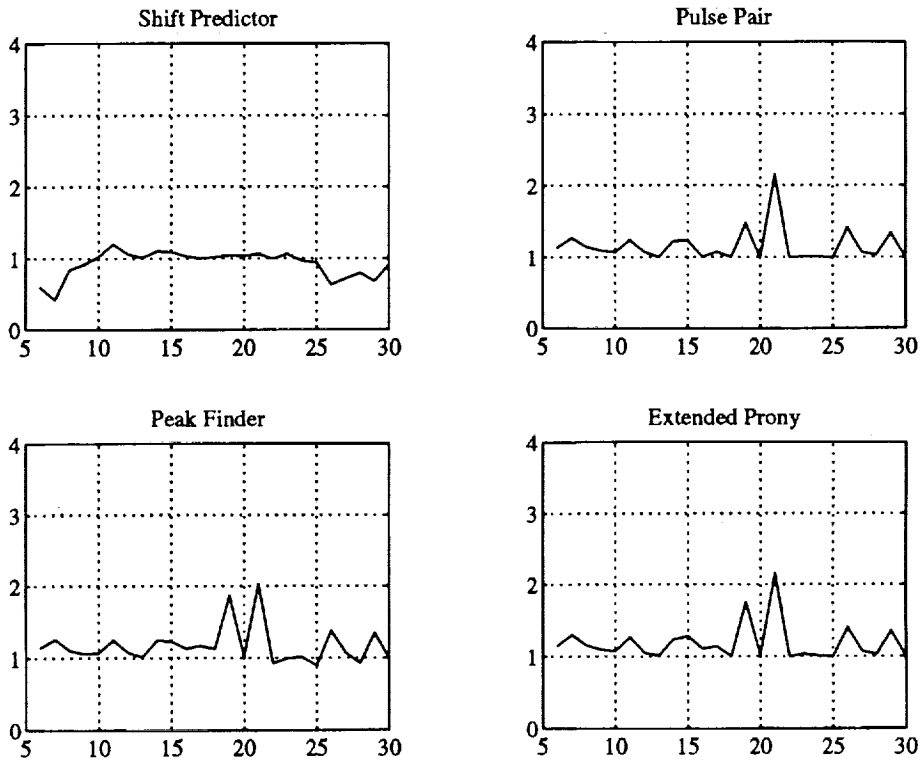

Figure 5.12 Clutter Rejection Factors for Complex Filtering of Frame 270

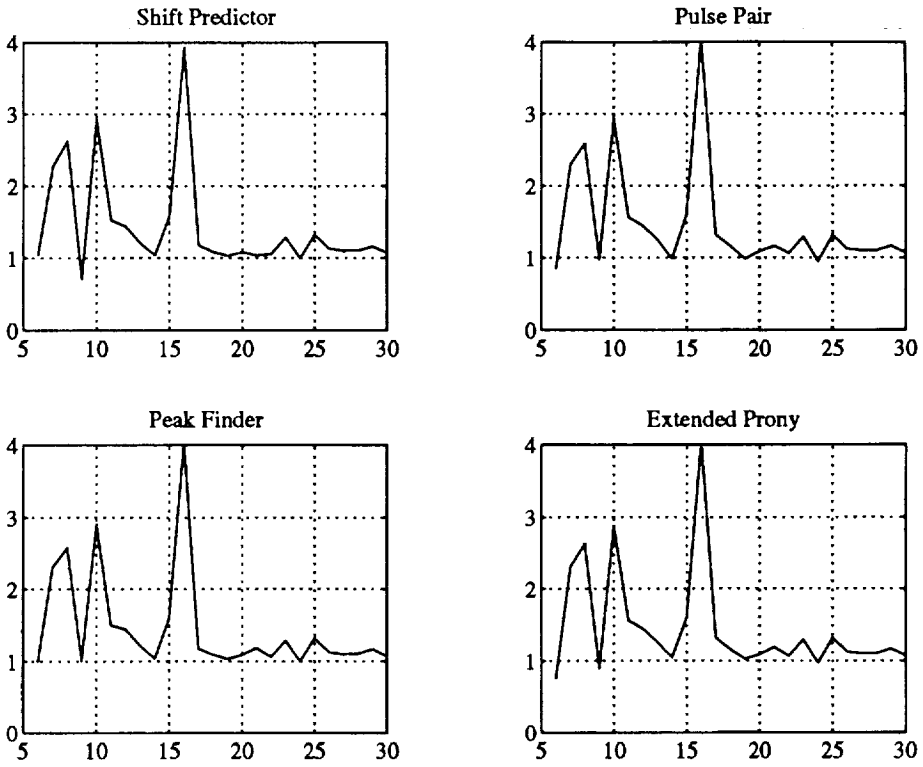

Figure 5.13 Clutter Rejection Factors for Complex Filtering of Frame 320

clutter gain of all of the filters show a greater attenuation when the dominant mode is present.

An important factor to consider is whether the improved clutter rejection is worth the added computational load necessary to implement the complex filtering scheme. Although at farther ranges the clutter gain of filtering shows a greater attenuation, the decreased attenuation at closer ranges is partly due to the fact that the signal level in these ranges is already low. A more important factor at the closer ranges is the "whiteness" of the clutter spectra. From the range cell spectra of Frame 270 in Appendix B, the closer range cells show a lack of any spectral mode. Since there is no dominant mode, filtering at different Doppler frequencies does not result in any improvement in clutter rejection. With the low power level and the spectral whiteness in the closer range cells, the computation necessary to search for a possibly nonexistent clutter mode does not seem to be a worthwhile cost. Thus the fixed notch at zero Doppler is probably a better choice.

CHAPTER 6

CONCLUSIONS

The ability of an airborne radar to correctly identify desired targets is very closely tied to its ability to successfully reject the clutter that appears in the return signal. For an airborne weather radar in the "lookdown" position, the strongest clutter return will be from the ground. Since the most common form of clutter rejection filter is a filter with a rejection notch centered at zero Doppler frequency (aircraft groundspeed), the successful rejection of ground clutter power depends on the ability of the receiver to center the clutter spectrum at zero frequency.

In theory there should be a main lobe clutter shift at close ranges based on the way the return spectrum is centered. For ranges less than the antenna boresight range to the ground, the dominant clutter is from sidelobes and is shifted away from the aircraft groundspeed. Since this shift is due to returns outside of the main lobe of the radar beam, the clutter returns at short ranges are attenuated by the reduced antenna gain. Because the clutter is at such a relatively low level, this predicted clutter shift should not be a real problem for the conventional clutter rejection filter.

For a lookdown radar centering is accomplished based on the antenna azimuth and tilt angles. When a clutter mode shift due to sidelobe returns occurs, there are at least three options which can be taken to possibly improve clutter rejection. One option is to center the clutter mode by using the complex demodulation process to shift the entire spectrum. After filtering with a zero centered notch filter, the entire spectrum would need to be shifted back to its original position in order to remove possible aliasing effects. Such a procedure requires a method of estimating the shift of the clutter mode.

A second option which is the topic of this study is to use a filter with complex coefficients which allows for the capability of locating the filter notch at the Doppler

position of the main clutter mode. The design of the complex coefficient filter is a simple procedure. It turns out that the majority of the computation time is spent on figuring out where to move the filter notch. Presented were three shift estimators and one predictor. The shift predictor bases its estimation of the shift location on the position data of the aircraft and the radar antenna. Such a predictive estimation is limited by the theory that the aircraft and antenna positioning are the only variables involved in the clutter mode shift, which cannot be proven to be true. The three shift estimators are the peak finder, the pulse pair estimator, and the extended Prony analysis, and while each has its drawbacks, they all do a fairly good job of tracking the clutter mode.

The complex filter is a simple tool which could be useful in other applications. The use of the complex filter in the rejection of discrete clutter could be effective depending on the algorithm for identifying such clutter. The principles of the extended Prony analysis seem to have potential use for clutter rejection filtering and possibly even for discrete clutter rejection. It would appear that increasing the AR model to at least order 3 could possibly allow for the identification of discrete clutter based on the logic used in previous research [6]. Further investigation would be necessary in order to find out if such a theory is feasible.

Another possible option for the compensation of the clutter mode shift is to implement a filter with a varying notch width. The width of the clutter rejection filter could be dependent on the spread of the clutter spectra. Such a variable width filter could even be implemented in conjunction with a complex filter. The use of such a filter in the rejection of clutter power is a topic for future study.

APPENDICES

Appendix A

Levinson–Durbin Algorithm

Autoregressive (AR) modeling has been recognized as an appropriate means of modeling the clutter in the airport terminal area. A study performed by Keel [11] investigates the use of the AR process to support an adaptive clutter rejection filtering scheme. Using the AR model for spectral estimation has been popular due to its relatively low computational load required and an improved spectral resolution over conventional FFT approaches. An AR model is an all pole model with the spectral density

$$\mathcal{P}_{AR}(f) = \frac{\sigma^2 \Delta t}{\left| 1 + \sum_{i=1}^{p} a_i \exp(-j2\pi f i \Delta t) \right|^2} \tag{A.1}$$

where Δt is the sampling interval of the process, $\{a_i\}$ are the AR coefficients, and σ^2 is the variance of the input white noise process. For a model of order p, the estimation of the parameters $\{a_1, a_2, \ldots, a_p, \sigma^2\}$ is required where it is possible for p to be any positive integer. One method of estimating these parameters is the Levinson–Durbin algorithm which is an efficient method of solving a matrix equation.

The Yule–Walker equations relate the coefficients $\{a_i\}$ of the AR model to the autocorrelation process of the signal $R_{xx}(k)$ [33]. The AR coefficients can be obtained by solving

$$\begin{array}{rcll} R_{xx}(k) & = & -\sum_{i=1}^{N} a_i R_{xx}(k-i) + \sigma^2 & k = 0 \\ R_{xx}(k) & = & -\sum_{i=1}^{N} a_i R_{xx}(k-i) & 1 \leq k \leq N \end{array} \tag{A.2}$$

which in matrix form is described by

$$\begin{bmatrix} R_{xx}(0) & R_{xx}(-1) & \cdots & R_{xx}(-p) \\ R_{xx}(1) & R_{xx}(0) & \cdots & R_{xx}(-(p-1)) \\ & & \vdots & \\ R_{xx}(p) & R_{xx}(p-1) & \cdots & R_{xx}(0) \end{bmatrix} \begin{bmatrix} 1 \\ a_1 \\ \vdots \\ a_p \end{bmatrix} = \begin{bmatrix} \sigma^2 \\ 0 \\ \vdots \\ 0 \end{bmatrix}. \tag{A.3}$$

The autocorrelation estimate $R_{xx}(k)$ of the complex series x_n is given by

$$R_{xx}(k) = \frac{1}{N} \sum_{n=0}^{N-k-1} x_{n+k} x_n^* \tag{A.4}$$

The Levinson–Durbin algorithm uses a recursive method of solving for the parameter set of the desired order model. For the pth order model the parameter set is $\{a_{p1}, a_{p2}, \ldots, a_{pp}, \sigma_p^2\}$ where a_{ki} refers to the ith coefficient of a kth order model. Starting with the first order parameters

$$\begin{aligned} a_{11} &= -\frac{R_{xx}(1)}{R_{xx}(0)} \\ \sigma_1^2 &= (1 - |a_{11}|^2) R_{xx}(0) \end{aligned} \tag{A.5}$$

the higher order parameters are recursively computed by the following:

$$\begin{aligned} a_{kk} &= -\frac{1}{\sigma_{k-1}^2} \left[R_{xx}(k) + \sum_{l=1}^{k-1} R_{xx}(k-l) \right] \\ a_{ki} &= a_{k-1,i} + a_{kk} a_{k-1,k-i}^* \\ \sigma_k^2 &= (1 - |a_{kk}|^2) \sigma_{k-1}^2 \ . \end{aligned} \tag{A.6}$$

By recursively solving for the model coefficients, the Levinson–Durbin algorithm gives the coefficients for all order models up to the desired order.

Appendix B

Range Cell Frequency Plots for Frame 270

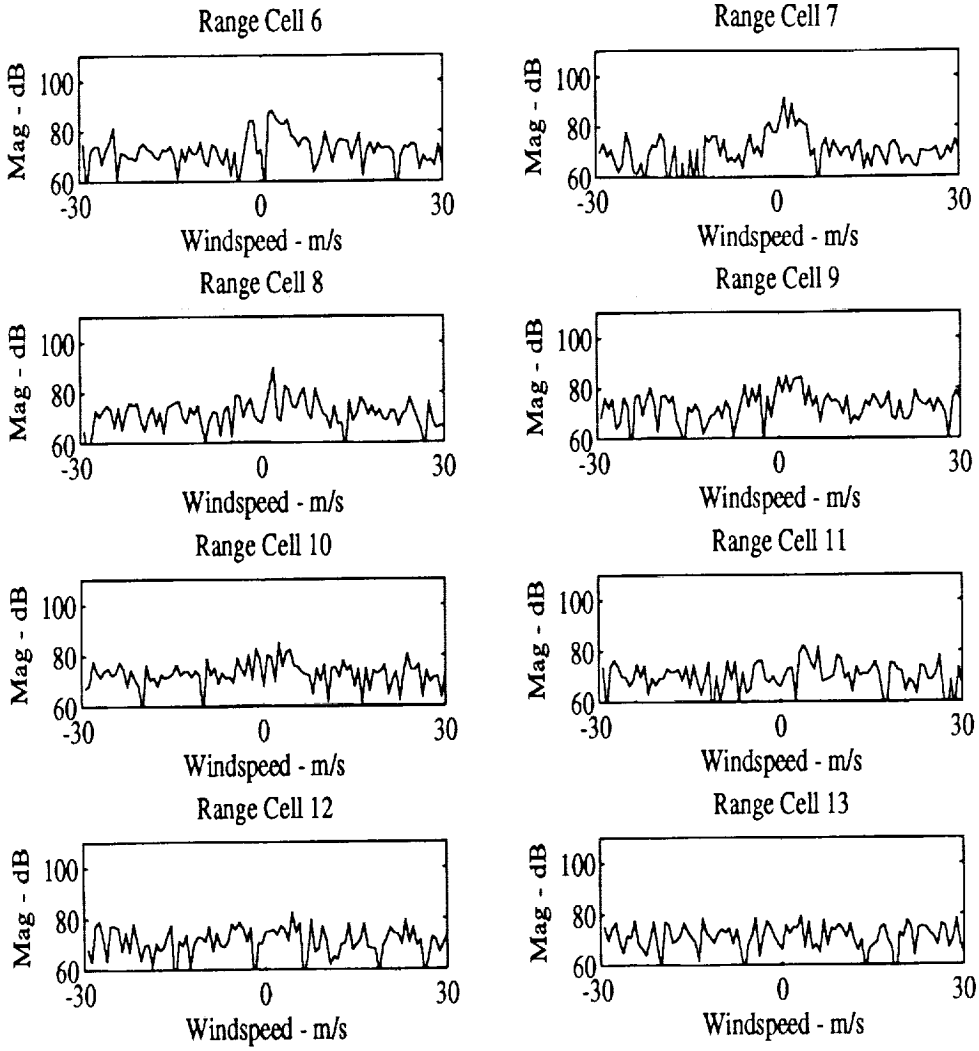

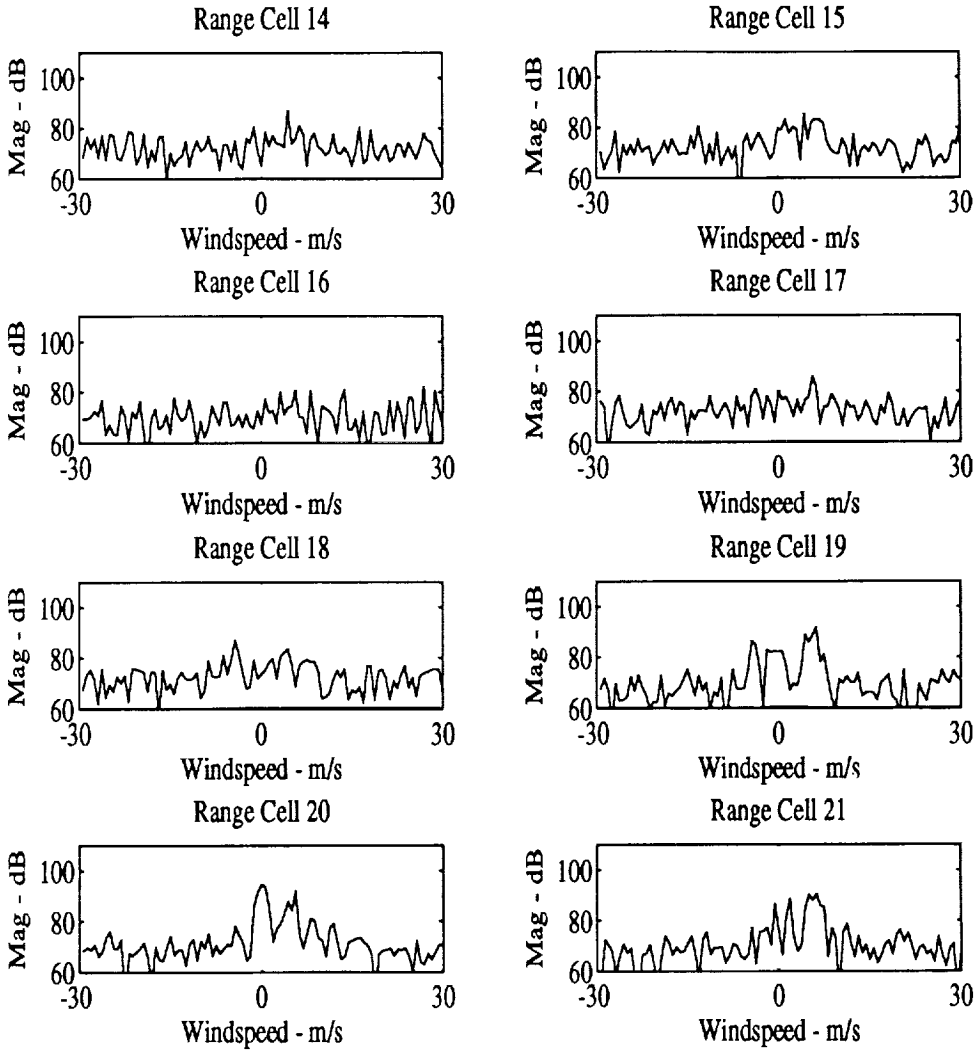
Range Cell 14
Range Cell 15
Range Cell 16
Range Cell 17
Range Cell 18
Range Cell 19
Range Cell 20
Range Cell 21
Mag - dB
100
80
60
-30
0
30
Windspeed - m/s

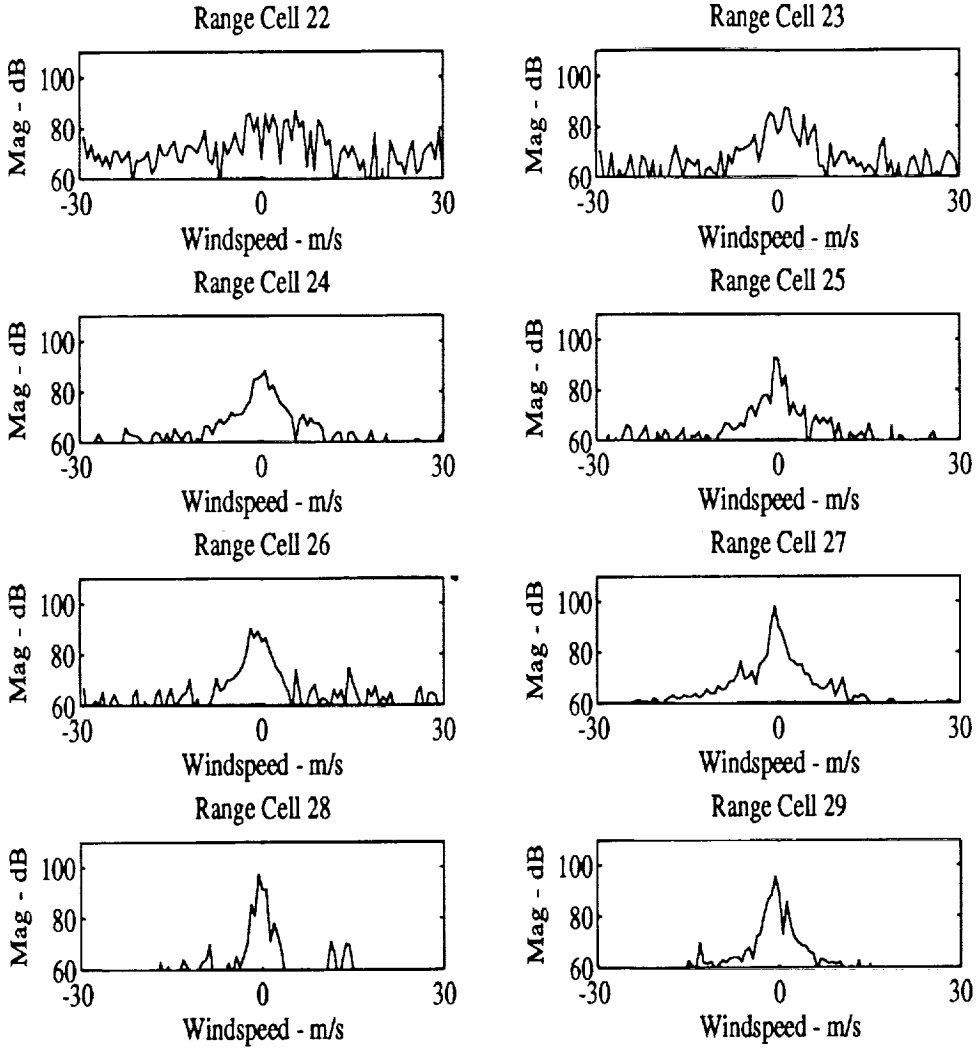
Range Cell 22
Range Cell 23
Range Cell 24
Range Cell 25
Range Cell 26
Range Cell 27
Range Cell 28
Range Cell 29
Mag - dB
100
80
60
-30
0
30
Windspeed - m/s

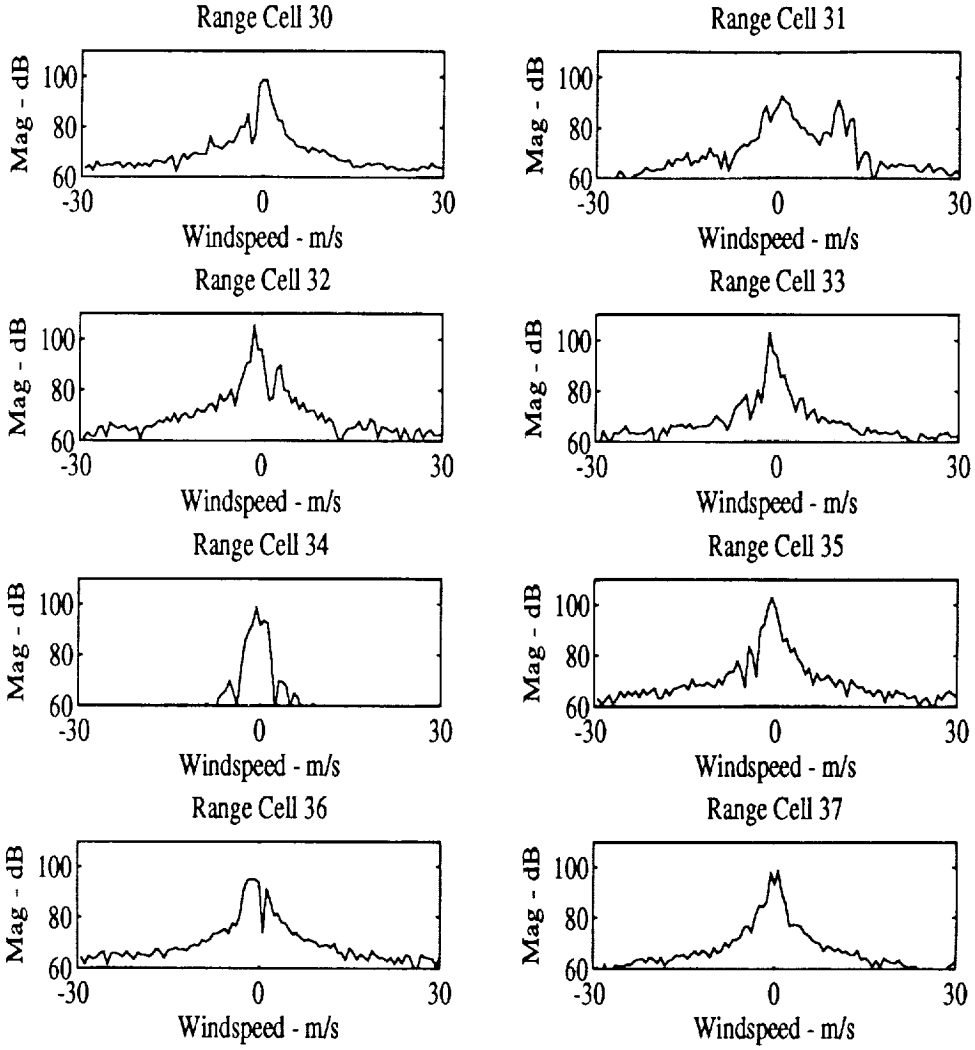
Range Cell 30
Range Cell 31
Range Cell 32
Range Cell 33
Range Cell 34
Range Cell 35
Range Cell 36
Range Cell 37
Mag - dB
100
80
60
-30
0
30
Windspeed - m/s

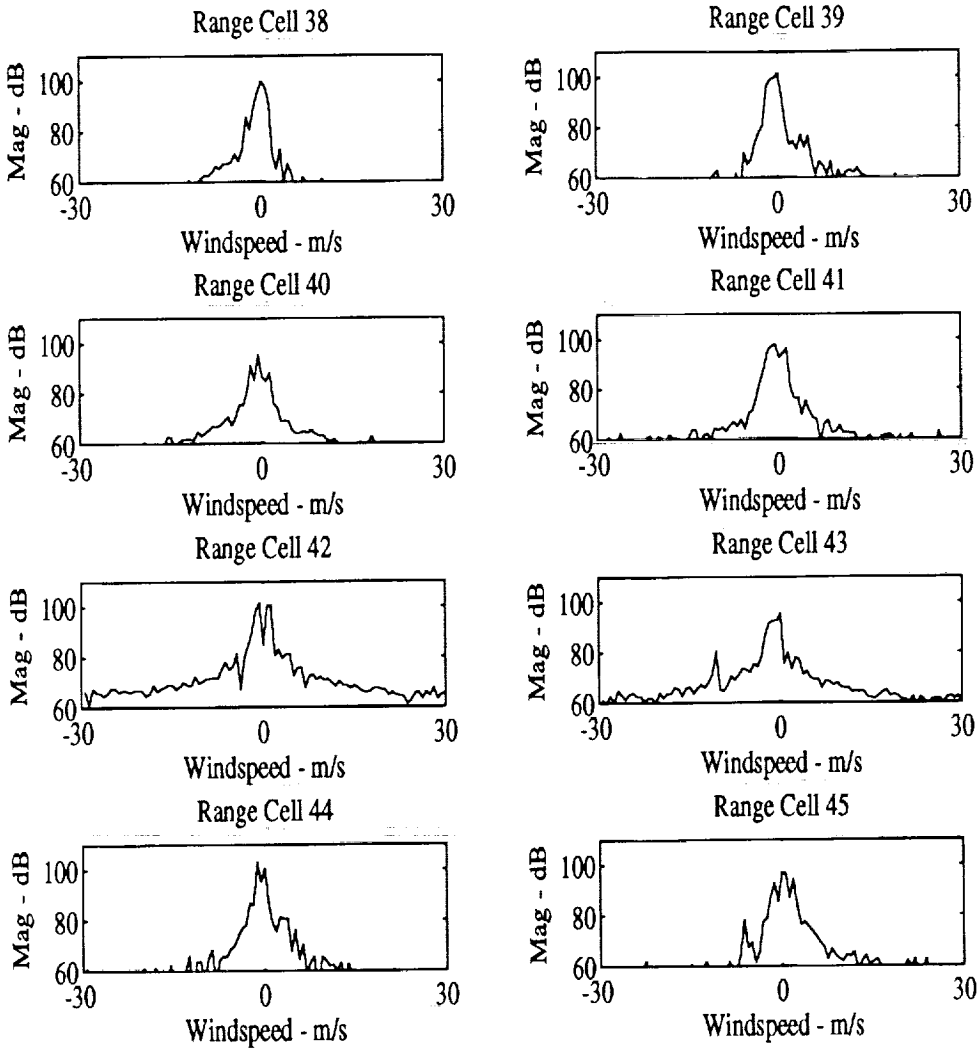
Range Cell 38
Range Cell 39
Range Cell 40
Range Cell 41
Range Cell 42
Range Cell 43
Range Cell 44
Range Cell 45
Mag - dB
100
80
60
-30
0
30
Windspeed - m/s

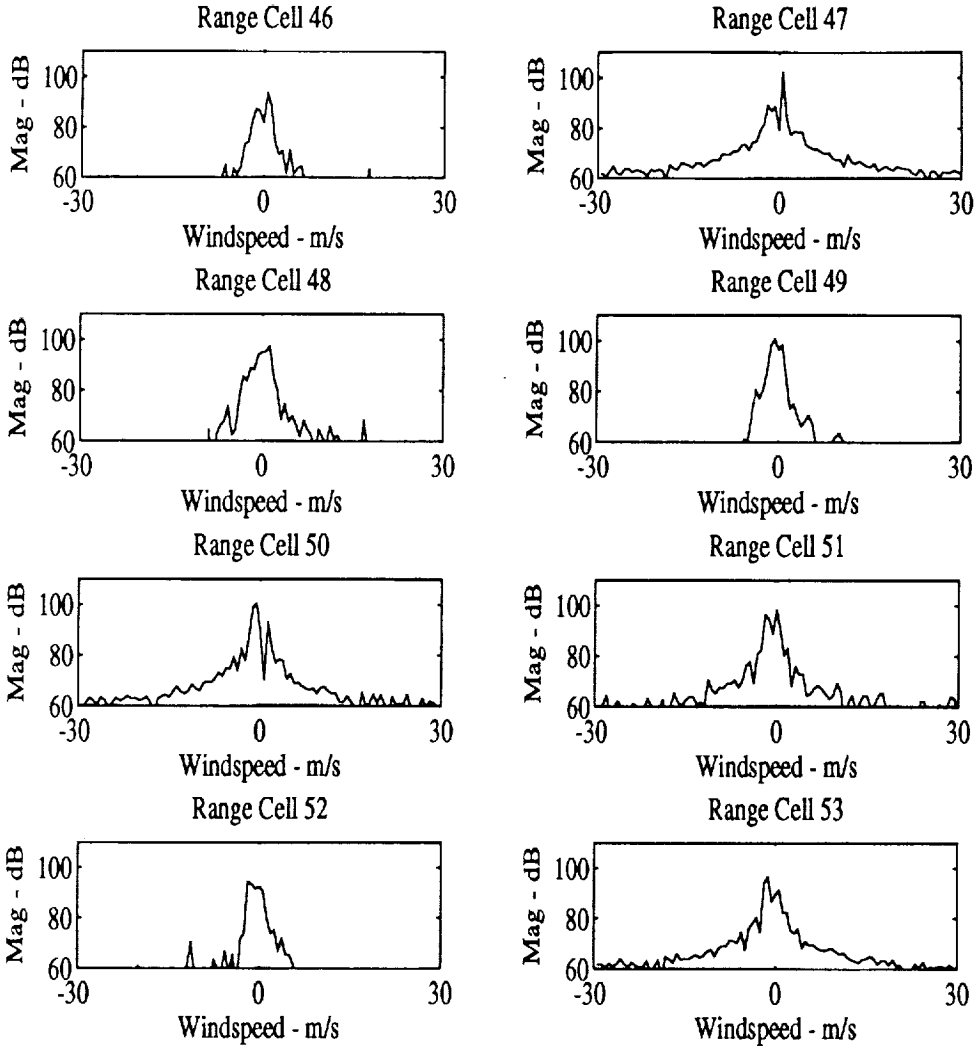
Range Cell 46
Range Cell 47
Range Cell 48
Range Cell 49
Range Cell 50
Range Cell 51
Range Cell 52
Range Cell 53
Mag - dB
100
80
60
-30
0
30
Windspeed - m/s

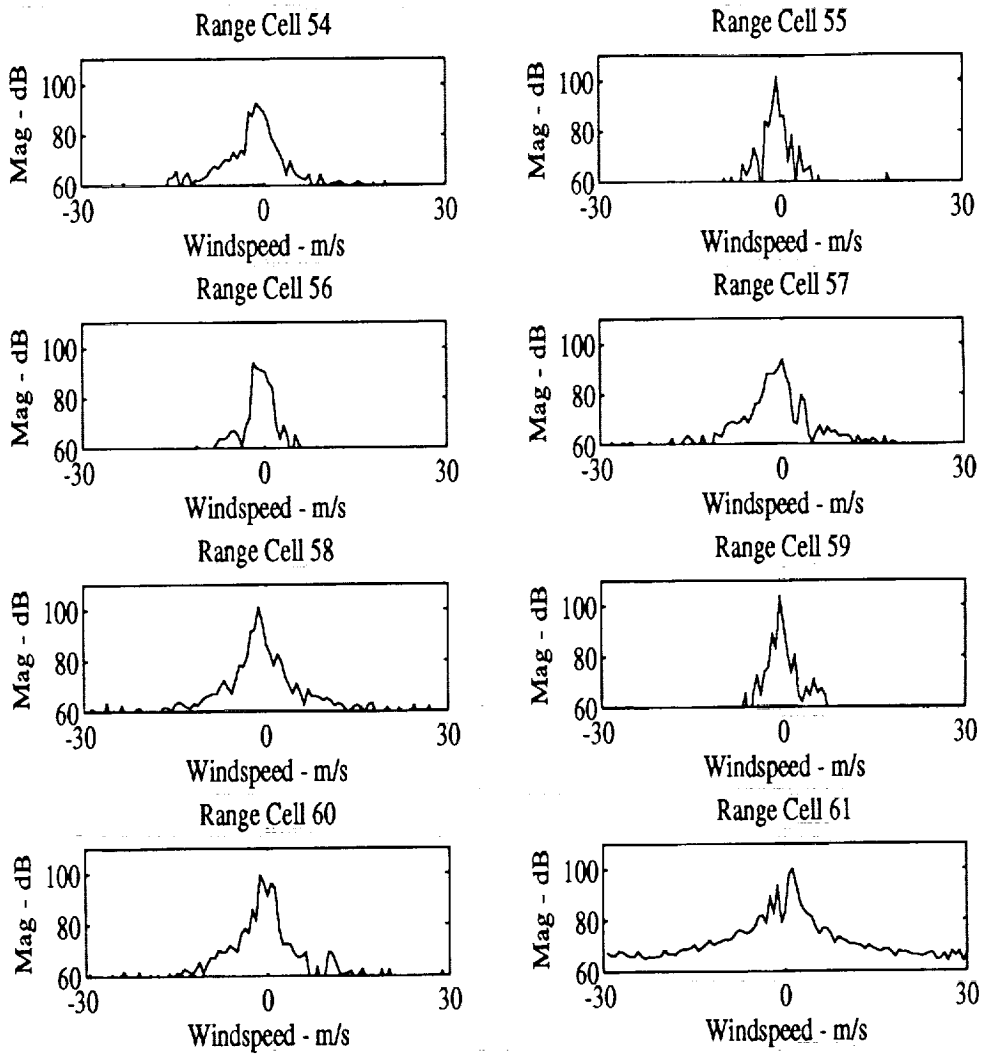
Range Cell 54
Range Cell 55
Range Cell 56
Range Cell 57
Range Cell 58
Range Cell 59
Range Cell 60
Range Cell 61
Mag - dB
100
80
60
-30
0
30
Windspeed - m/s

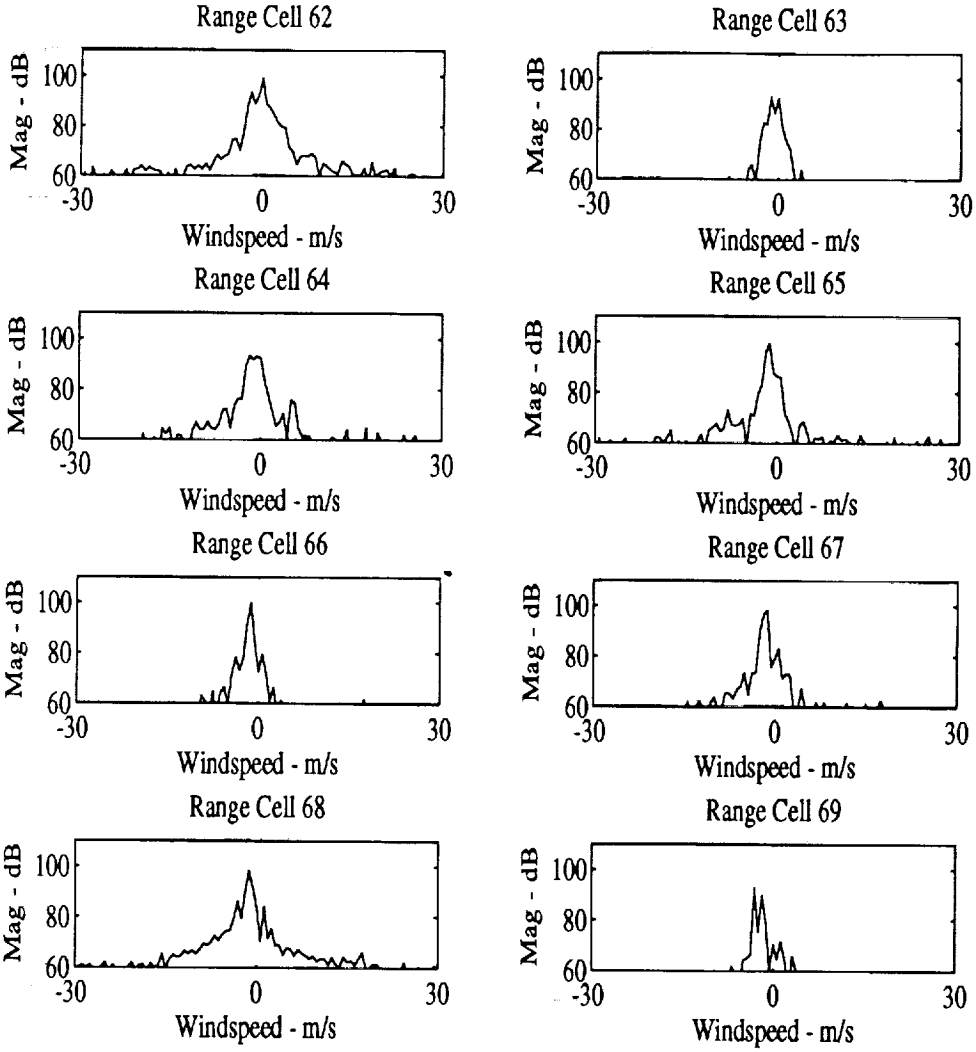
Range Cell 62
Range Cell 63
Range Cell 64
Range Cell 65
Range Cell 66
Range Cell 67
Range Cell 68
Range Cell 69
Mag - dB
100
80
60
-30
0
30
Windspeed - m/s

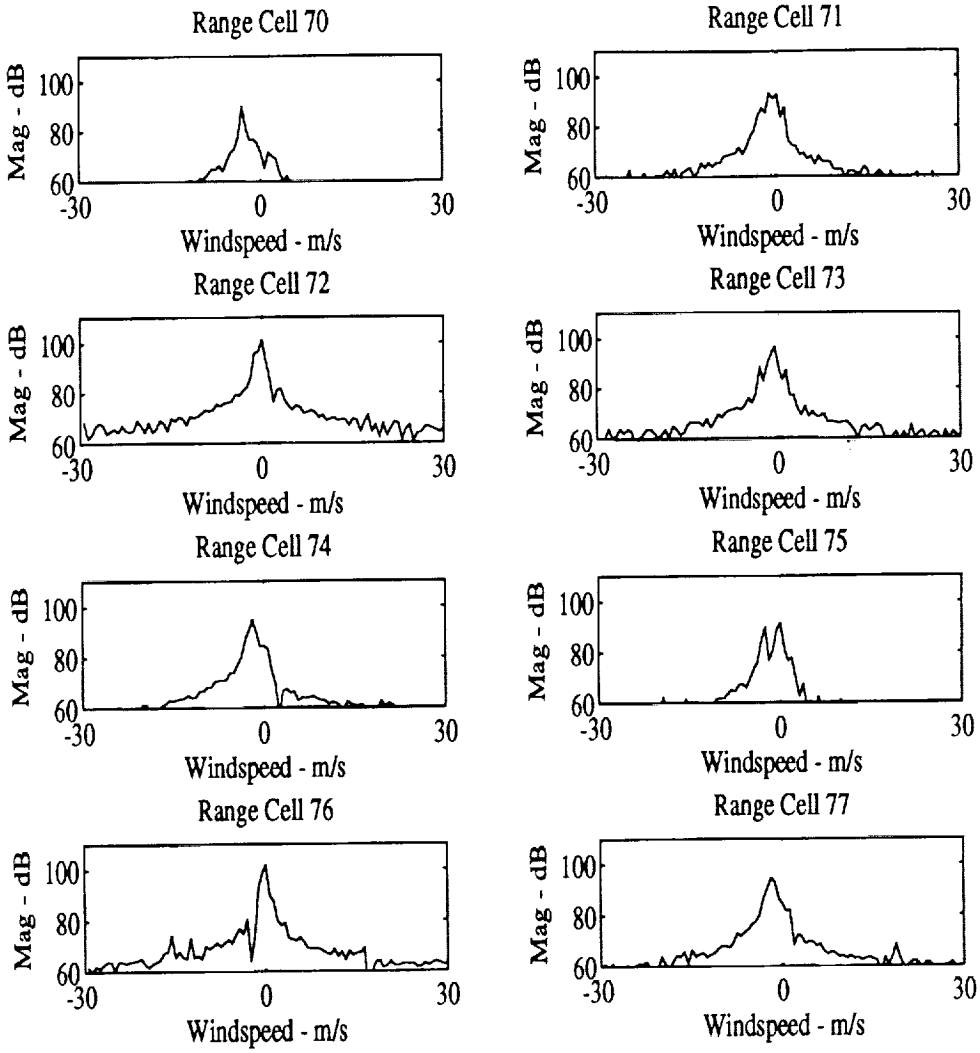
Range Cell 70
Mag - dB
100
80
60
-30
0
30
Windspeed - m/s
Range Cell 71
Mag - dB
100
80
60
-30
0
30
Windspeed - m/s
Range Cell 72
Mag - dB
100
80
60
-30
0
30
Windspeed - m/s
Range Cell 73
Mag - dB
100
80
60
-30
0
30
Windspeed - m/s
Range Cell 74
Mag - dB
100
80
60
-30
0
30
Windspeed - m/s
Range Cell 75
Mag - dB
100
80
60
-30
0
30
Windspeed - m/s
Range Cell 76
Mag - dB
100
80
60
-30
0
30
Windspeed - m/s
Range Cell 77
Mag - dB
100
80
60
-30
0
30
Windspeed - m/s

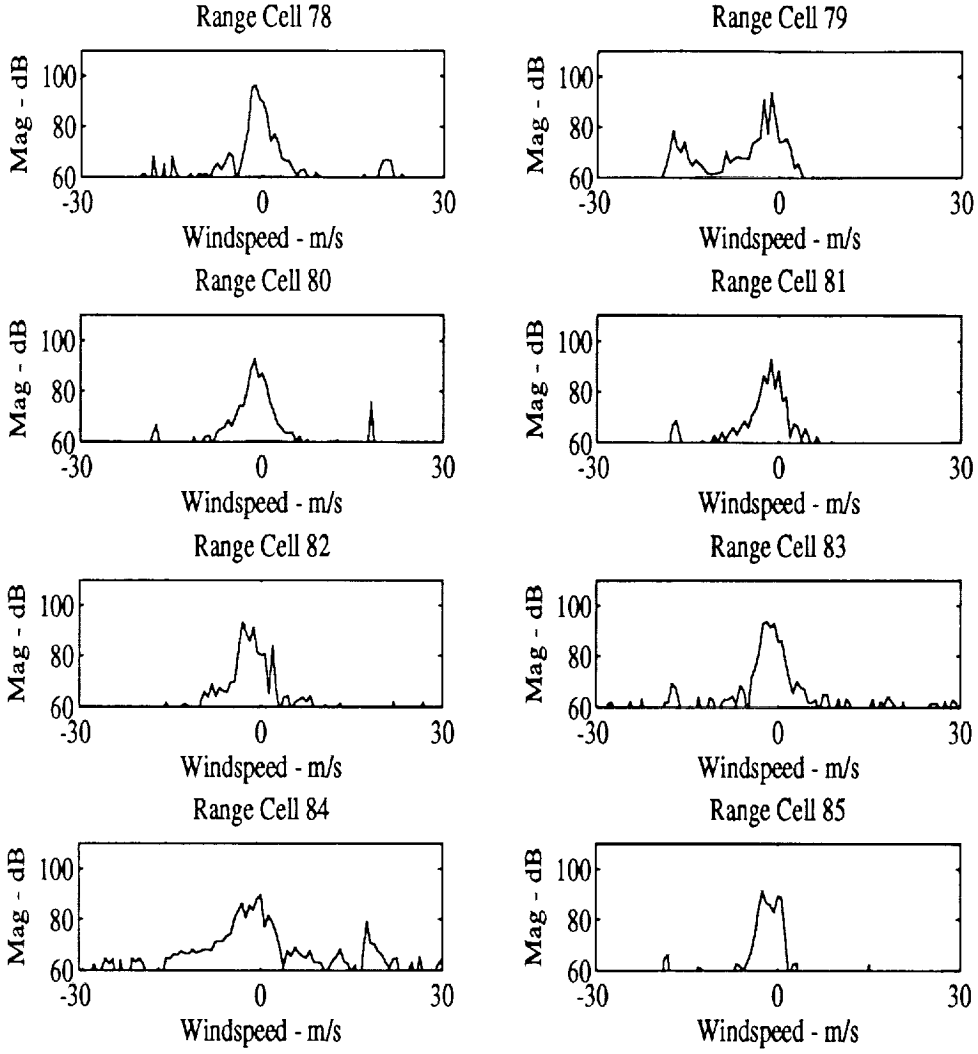
Range Cell 78
Range Cell 79
Range Cell 80
Range Cell 81
Range Cell 82
Range Cell 83
Range Cell 84
Range Cell 85
Mag - dB
100
80
60
-30
0
30
Windspeed - m/s

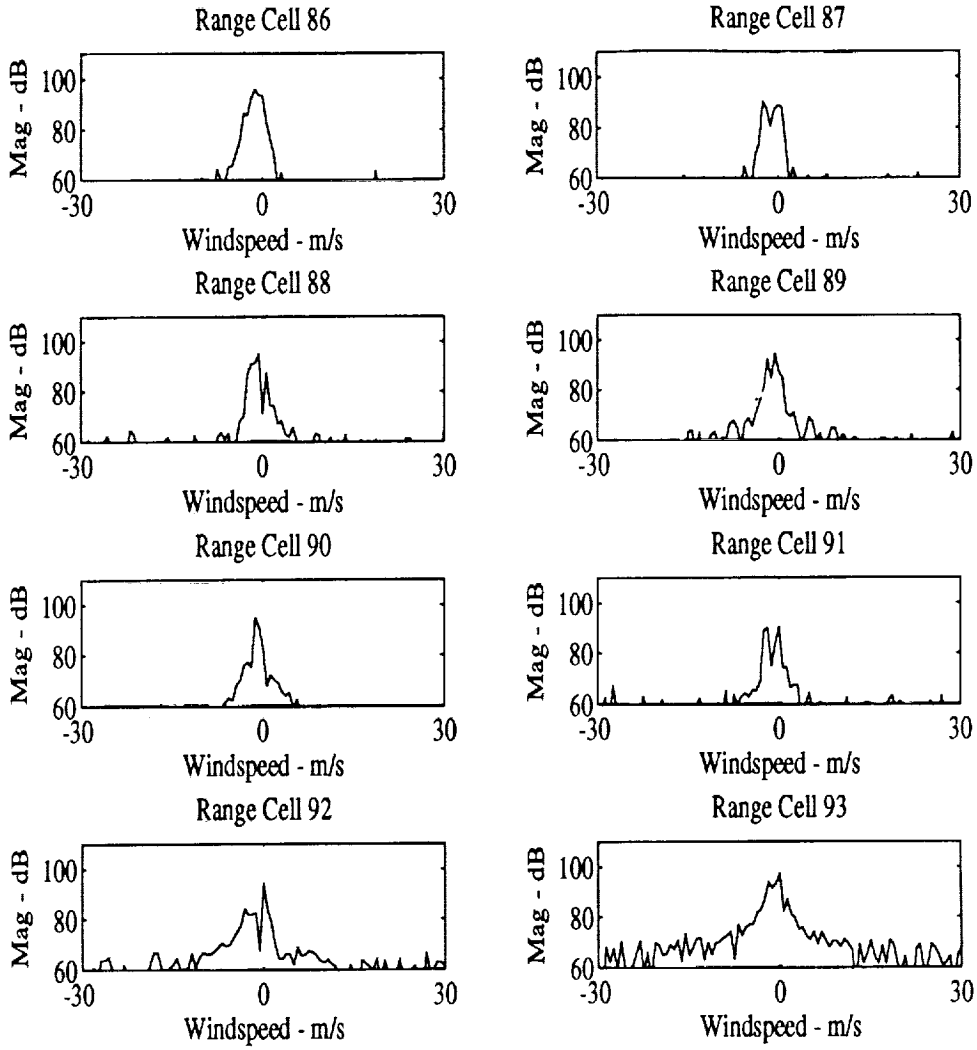
Range Cell 86
Range Cell 87
Range Cell 88
Range Cell 89
Range Cell 90
Range Cell 91
Range Cell 92
Range Cell 93
Mag - dB
100
80
60
-30
0
30
Windspeed - m/s

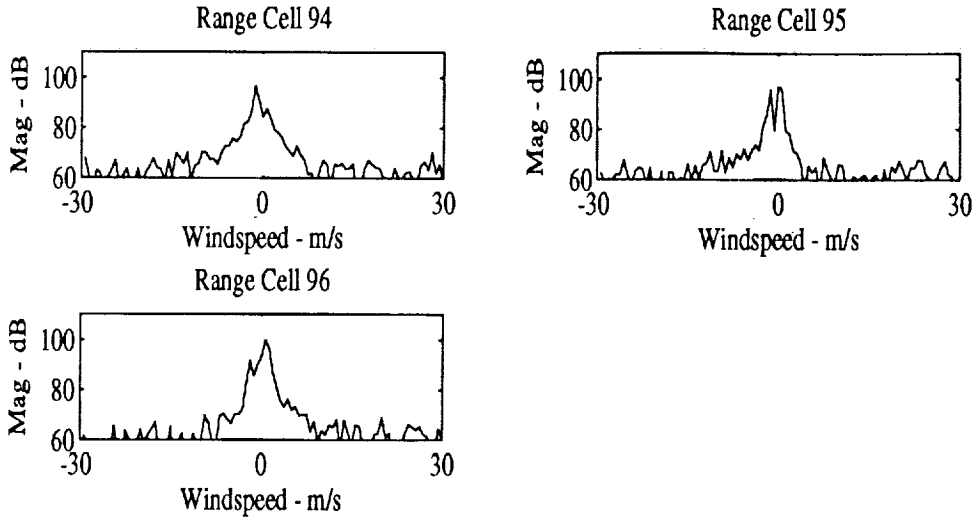
Range Cell 94
Mag - dB
100
80
60
-30
0
30
Windspeed - m/s
Range Cell 95
Mag - dB
100
80
60
-30
0
30
Windspeed - m/s
Range Cell 96
Mag - dB
100
80
60
-30
0
30
Windspeed - m/s

REFERENCES

1. M. I. Skolnik, editor. *Radar Handbook.* McGraw-Hill, New York, 1990.

2. G. V. Morris, editor. *Airborne Pulsed Doppler Radar.* Artech House, Norwood, Massachusetts, 1988.

3. S. A. Hovanessian. "Medium PRF Performance Analysis". *IEEE Trans. on Aerospace and Electronic Systems*, vol. AES-18, May 1982, pp. 286–296.

4. W. W. Shrader and V. G. Hansen. "New Clutter Rejection Waveforms for Long-Range Radar". *IEEE Trans. on Aerospace and Electronic Systems*, vol. AES-16, November 1980, pp. 763–770.

5. F. W. Sears, M. W. Zemansky, and Young H. D. *University Physics.* Addison-Wesley, Reading, Massachusetts, 1987.

6. M. W. Kunkel. "Spectrum Modal Analysis for the Detection of Low-Altitude Windshear With Airborne Radar". NASA CR-4457, August 1992.

7. W. T. Davis. "The Effects of Clutter-Rejection Filtering on Estimating Weather Spectrum Parameters". NASA CR-186212, July 1989.

8. D. S. Zrnić. Estimation of spectral moments for weather echoes. *"IEEE Transactions on Geoscience Electronics"*, vol. GE-17, 1979, pp. 113–128.

9. E. G. Baxa, Jr. and J. Lee. "The Pulse Pair Algorithm as a Robust Estimator of Turbulent Weather Spectral Parameters Using Airborne Pulse Doppler Radar". NASA CR-186792, February 1991.

10. D. D. Aalfs. "Real Time Processing of Radar Return on a Parallel Computer". NASA CR-4456, July 1991.

11. B. M. Keel. "Adaptive Clutter Rejection Filters for Airborne Doppler Weather Radar Applied to the Detection of Low Altitude Windshear". NASA CR-186211, December 1989.

12. E. G. Baxa, Jr. "Airborne Pulsed Doppler Radar Detection of Low-Altitude Windshear — A Signal Processing Problem". *Digital Signal Processing*, vol. 1, no. 4, October 1991, pp. 186–197.

13. E. Bracalente. "Doppler Radar Results". *NASA Conference Publication 10105, DOT/FAA/RD-92/19-I*, September 1992, pp. 115–140.

14. C. L. Britt. "Algorithm to Complensate for Clutter Velocity Offset in the Windshear Radar". Tech. Memo. Project 3042-68, Research Triangle Institute, Research Triangle Park, North Carolina, June 1989.

15. Y. C. Lai and E. G. Baxa, Jr. "On the Application of the LMS–Based Adaptive Noise Canceller in Nonstationary Environment Associated with Airborne Doppler Weather Radar". In *Proc. of 1993 IEEE Int. Conf. on Acoustics, Speech, and Signal Processing*, Minneapolis, April 1993.

16. L. C. Ludeman. *Fundamentals of Digital Signal Processing.* Harper and Row, New York, 1986.

17. A. V. Oppenheim and R. W. Schafer. *Discrete-Time Signal Processing.* Prentice Hall, Englewood Cliffs, New Jersey, 1989.

18. T. H. Crystal and L. Ehrman. "The Design and Applications of Digital Filters with Complex Coefficients". *IEEE Transactions on Audio and Electroacoustics*, vol. AU-16, September 1968, pp. 315–320.

19. H. Iwakura. "New Frequency Transformations for Complex Digital Filters". *Electronics Letters*, vol. 27, October 1991, pp. 2083–2085.

20. P. A. Regalia, S. K. Mitra, and J. Fadavi-Ardekani. "Implementation of Real Coefficient Digital Filters Using Complex Arithmetic". *IEEE Transactions on Circuits and Systems*, vol. CAS-34, 1987, pp. 345–353.

21. W. L. Mills, C. T. Mullis, and R. A. Roberts. "Digital Filter Realizations Without Overflow Oscillations". *IEEE Transactions on Accoust., Speech Signal Process.*, vol. ASSP-26, August 1978, pp. 334–338.

22. T. T. Fujita. "The Downburst". SMRP Research Paper No. 210, The University of Chicago, 1985. (available from NTIS as PB85-148-880).

23. M. Eide and B. Mathews. "Acquisition and Use of Orlando, Florida and Continental Airbus Radar Flight Test Data". *NASA Conference Publication 10105, DOT/FAA/RD-92/19-I*, September 1992, pp. 357–372.

24. R. L. Bowles and R. Targ. "Windshear Detection and Avoidance: Airborne Systems Perspective". Presented at the 16^{th} Congress of the ICAS, Jerusalem, Israel, August 28 – September 2, 1988.

25. R. E. Bach and R. C. Wingrove. "Analysis of Windshear from Airline Flight Data". *J. Aircr.*, vol. 26, February 1989, pp. 103–109.

26. W. H. Heiss, D. L. McGrew, and D. Sirmans. "Nexrad: Next Generation Weather Radar (WSR–88D)". *Microwave Journal*, January 1990, pp. 79–98.

27. M. Michelson, W. W. Shrader, and J. G. Wieler. "Terminal Doppler Weather Radar". *Microwave Journal*, February 1990, pp. 139–148.

28. J. Evans and D. Turnbull. "Development of an Automated Windshear Detection System Using Doppler Weather Radar". *Proceedings of the IEEE*, vol. 77, no. 11, November 1989, pp. 1661–1673.

29. J. McCarthy. "Advances in Weather Technology for the Aviation System". *Proceedings of the IEEE*, vol. 77, no. 11, November 1989, pp. 1728–1734.

30. S. Campbell, A. Berke, and M. Matthews. "The Orlando TDWR Testbed and Airborne Wind Shear Data Comparison Results". *NASA Conference Publication 10105, DOT/FAA/RD-92/19-II*, September 1992, pp. 811–846.

31. A. I. Mackenzie, E. G. Baxa, Jr., and S. D. Harrah. "Characterization of Urban Ground Clutter with New Generation Airborne Doppler Weather Radar". In *Proceedings of 1993 IEEE National Radar Conference*, Boston, April 1993.

32. S. Haykin, B. W. Currie, and S. Kessler. "Maximum Entropy Spectral Analysis of Radar Clutter". *Proceedings of the IEEE*, vol. 70, September 1982, pp. 953–962.

33. S. M. Kay and S. L. Marple. "Spectrum Analysis—A Modern Perspective". *Proceedings of the IEEE*, vol. 69, no. 11, November 1981, pp. 1380–1419.

REPORT DOCUMENTATION PAGE

Form Approved
OMB No. 0704-0188

1. AGENCY USE ONLY (Leave blank)	2. REPORT DATE	3. REPORT TYPE AND DATES COVERED
	October 1993	Contractor Report

4. TITLE AND SUBTITLE
Designing Clutter Rejection Filters with Complex Coefficients for Airborne Pulsed Doppler Weather Radar

5. FUNDING NUMBERS
WU 505-64-12-02

G NAG1-928

6. AUTHOR(S)
Dennis A. Jamora

7. PERFORMING ORGANIZATION NAME(S) AND ADDRESS(ES)
Radar Systems Laboratory
Electrical and Computer Engineering Department
Clemson University
Clemson, SC 29634-0915

8. PERFORMING ORGANIZATION REPORT NUMBER
Technical Report #16

9. SPONSORING / MONITORING AGENCY NAME(S) AND ADDRESS(ES)
National Aeronautics and Space Administration
Langley Research Center
Hampton, VA 23681-0001

10. SPONSORING / MONITORING AGENCY REPORT NUMBER
NASA CR-4550
DOT/FAA/RD-93/24

11. SUPPLEMENTARY NOTES
Langley Technical Monitor: Anne I. Mackenzie
Final Report

12a. DISTRIBUTION / AVAILABILITY STATEMENT
Unclassified - Unlimited

Subject Category 03

12b. DISTRIBUTION CODE

13. ABSTRACT *(Maximum 200 words)*

Ground clutter interference is a major problem for airborne pulse Doppler radar operating at low altitudes in a look-down mode. With Doppler zero set at the aircraft ground speed, ground clutter rejection filtering is typically accomplished using a high-pass filter with real valued coefficients and a stopband notch centered at zero Doppler. Clutter spectra from the NASA Wind Shear Flight Experiments of 1991-1992 show that the dominant clutter mode can be located away from zero Doppler, particularly at short ranges dominated by sidelobe returns. This report investigates use of digital notch filters with complex valued coefficients so that the stopband notch can be located at any Doppler frequency. Several clutter mode tracking algorithms are considered to estimate the Doppler frequency location of the dominant clutter mode. From the examination of flight data, when a dominant clutter mode away from zero Doppler is present, complex filtering is able to significantly increase clutter rejection over use of a notch filter centered at zero Doppler.

14. SUBJECT TERMS
Doppler radar, clutter filtering, complex coefficients, airborne weather radar

15. NUMBER OF PAGES
88

16. PRICE CODE
A05

17. SECURITY CLASSIFICATION OF REPORT	18. SECURITY CLASSIFICATION OF THIS PAGE	19. SECURITY CLASSIFICATION OF ABSTRACT	20. LIMITATION OF ABSTRACT
Unclassified	Unclassified	Unclassified	